

A Parameter Privacy-Preserving Strategy for Mixed-Autonomy Platoon Control

Jingyuan Zhou^a, Kaidi Yang^{a,*}

^aDepartment of Civil and Environmental Engineering, National University of Singapore, 1 Engineering Drive 2, Singapore, 117576, Singapore

ARTICLE INFO

Keywords:

Connected and Automated Vehicles
Mixed-Autonomy Platoon Control
Leading Cruise Control
Parameter Privacy Filter
String Stability

ABSTRACT

It has been demonstrated that leading cruise control (LCC) can improve the operation of mixed-autonomy platoons by allowing connected and automated vehicles (CAVs) to make longitudinal control decisions based on the information provided by surrounding vehicles. However, LCC generally requires surrounding human-driven vehicles (HDVs) to share their real-time states, which can be used by adversaries to infer drivers' car-following behavior, potentially leading to financial losses or safety concerns. This paper aims to address such privacy concerns and protect the behavioral characteristics of HDVs by devising a parameter privacy-preserving approach for mixed-autonomy platoon control. First, we integrate a parameter privacy filter into LCC to protect sensitive car-following parameters. The privacy filter allows each vehicle to generate seemingly realistic pseudo states by distorting the true parameters to pseudo parameters, which can protect drivers' privacy in behavioral parameters without significantly influencing the control performance. Second, to enhance the practicality and reliability of the privacy filter within LCC, we first extend the current approach to accommodate continuous parameter spaces through a neural network estimator. Subsequently, we introduce an individual-level parameter privacy preservation constraint, focusing on the privacy level of each individual parameter pair, further enhancing the approach's reliability. Third, analysis of head-to-tail string stability reveals the potential impact of privacy filters in degrading mixed traffic flow performance. Simulation shows that this approach can effectively trade off privacy and control performance in LCC. We further demonstrate the benefit of such an approach in networked systems, i.e., by applying the privacy filter to a preceding vehicle, one can also achieve a certain level of privacy for the following vehicle.

1. Introduction

The transformative technology of connected and automated vehicles (CAVs) presents enormous potential in improving transportation systems (Yang et al., 2016; Li et al., 2017; Feng et al., 2018; Tilg et al., 2018; Guo et al., 2019; Zhou and Zhu, 2021; Woo and Skabardonis, 2021; Tan et al., 2022; Deng et al., 2023; Apostolakis et al., 2023). Significant research attention has been paid to the longitudinal control of CAVs within a platoon, thanks to the benefits of improving traffic capacity and stability. Early studies of CAV longitudinal control focus on cooperative adaptive cruise control (CACC) (Zhang et al., 2022; Dey et al., 2015; Xiao et al., 2018; Zhang et al., 2020), which coordinates a platoon of CAVs following a designed head vehicle. However, a long transition is expected to be needed to achieve full autonomy, and hence, CAVs and human-driven vehicles (HDVs) will coexist in the near future.

The key challenge associated with the control of mixed-autonomy platoons lies in the coordination of CAVs, considering the uncertain behavior of HDVs. Orosz (2016) and Shen et al. (2023) formulated and

*Corresponding author

✉ jingyuanzhou@u.nus.edu (J. Zhou); kaidi.yang@nus.edu.sg (K. Yang)
ORCID(s): 0000-0002-1201-3189 (J. Zhou); 0000-0001-5120-2866 (K. Yang)

proposed control strategies for connected cruise control, where CAVs can utilize the real-time information of the HDVs ahead of them. Later, Wang et al. (2021) introduced the notion of leading cruise control (LCC), which extends the classical cruise control by allowing CAVs to exploit the information of both leading and following HDVs. In LCC, a central unit (e.g., roadside unit or cloud) collects information from all vehicles in the platoon via vehicle-to-infrastructure (V2I) communications and calculates the optimal control input for CAVs. Various controllers have been proposed to implement LCC, including linear feedback controllers (Wang et al., 2021), optimization-based controllers (Chen et al., 2021), data-driven controllers (Wang et al., 2022b,a) and deep reinforcement learning-based controllers (Wang et al., 2023b; Zhou et al., 2024). These controllers have been demonstrated to be effective in improving string stability and reducing energy consumption while ensuring safety (Zhou and Yu, 2022; Zhou et al., 2024).

However, LCC requires both HDVs and CAVs to share real-time system states (e.g., positions and speeds) with the central unit, which can consequently store a long history of HDVs' shared states. Such data-sharing can impose privacy risks on these vehicles. The honest but curious central unit, or any adversaries who have access to the information stored on it, can exploit the received vehicle states to infer sensitive parameters characterizing HDVs' driving behavior in various traffic scenarios. The leakage of information on HDV driving patterns can lead to economic losses for drivers, as insurance companies can use these data to set discriminatory prices. In addition, malicious attackers may exploit these parameters to perform attacks on HDVs, which may compromise the safety of these drivers. Due to such concerns, HDVs may not be willing to participate in the system, which may reduce the amount of information the central unit can collect and hence undermine the benefits of LCC.

To the best of our knowledge, there has been no research on protecting sensitive system parameters of HDVs, especially in the context of mixed-autonomy platoon control. The existing literature considering vehicle privacy focuses on location privacy (Sun et al., 2013; Ma et al., 2019; Li et al., 2019; Cai et al., 2021; Qin et al., 2022; Pan et al., 2022; Zhang et al., 2023; Sun et al., 2023; Tsao et al., 2022a,b, 2023; Tan and Yang, 2024), i.e., protecting the location or location sequence of a vehicle from being accessed by adversaries. For example, Li et al. (2019) presented a Paillier cryptosystem-based platoon recommendation scheme for head vehicle selection, which effectively ranks head vehicles using user vehicle feedback, while preserving their location privacy. Pan et al. (2022) introduced a fault-tolerant encryption-decryption control strategy (Gao et al., 2021) designed for each vehicle within a platoon. This strategy can effectively preserve the privacy of individual vehicle data, such as location and velocity, while simultaneously ensuring the stability of the controller. Zhang et al. (2023) designed an affine masking-based privacy protection method in the LCC context to protect information from CAVs by transforming their true states and control signals via a low-dimensional affine transformation. However, the method proposed in this work can only be applied to controllers based on a specific controller, i.e., data-enabled predictive control (DeePC), and may not work together with other controllers. Moreover, although these works can preserve the privacy of vehicle locations, they do not necessarily prevent key system parameters from being inferred due to the law of large numbers (Nekouei et al., 2022). For example, adversaries can apply classical model identification methods (Teunissen, 1990; Wills and Ninness, 2008) such as Bayesian filters to estimate the key parameters with high confidence. Although He and Chow (2019) attempted to protect the privacy of sensitive parameters of Transportation Network Companies when they share trajectory data, their work considered only the parameters associated with a static optimization problem instead of the parameters of dynamical systems, which can be more challenging to protect due to the temporal dependence of the shared data.

To address the aforementioned gaps, in this paper, we integrate a statistical parameter privacy filter into the control of mixed-autonomy platoons to distort the information shared by HDVs to protect their car-following parameters. Our proposed method extends Nekouei et al. (2022), one of the few existing methodological tools to protect the privacy of sensitive parameters of dynamical systems, which generates seemingly realistic synthetic system states by distorting key parameters. Although the privacy filter proposed

in Nekouei et al. (2022) has been shown to be effective in various applications, such as protecting control gains in the Active Steering Control System (Nekouei et al., 2021), it suffers from three limitations. First, the privacy filter was developed for scenarios with small discrete parameter space and can be computationally inefficient if the parameter space is large or continuous, e.g., the car-following parameters in the case of mixed-autonomy platoon control. Second, the privacy guarantee provided by Nekouei et al. (2022) is for the entire distribution of the parameters rather than each possible value. In other words, the resulting privacy protection may be weak for drivers with specific parameters, especially if the parameters appear with a low probability, leading to fairness issues among drivers. Third, previous applications of the parameter privacy filter have not considered the trade-off between privacy and control performance in networked systems such as vehicle platoons, whereby the perturbations added to the states of one vehicle could influence the string stability of the platoon. To address the first two limitations, we extend Nekouei et al. (2022) by devising a learning-based privacy filter with an individual-level privacy preservation constraint, which can not only accelerate the computation but also provide the privacy guarantee for individual car-following parameters. To address the third limitation, we investigate the trade-offs associated with fuel consumption, velocity error, and head-to-tail string stability (Feng et al., 2019) in the mixed-autonomy platoon. The head-to-tail string stability analysis is conducted by constructing the head-to-tail transfer function under privacy filters' perturbations and string stable regions over different distorted sensitive parameters.

Statement of Contribution. The contribution of this paper is three-fold. First, we propose a parameter privacy-preserving strategy to protect the car-following parameters of HDVs from being inferred from their shared data in mixed-autonomy platoon control. This is one of the pioneering works on protecting the privacy of sensitive parameters associated with the dynamic operation of traffic systems. Unlike existing works that merely conceal or perturb vehicles' trajectory data, our approach can protect against inference attacks on sensitive parameters of vehicles' longitudinal driving behavior in mixed-autonomy platoons. Second, we propose a learning-based parameter privacy filter with an individual-level privacy preservation constraint to overcome the inability of the privacy filter to handle continuous parameter space and the potentially weak privacy-preserving performance when applied to specific sensitive parameters. This learning-based estimator efficiently processes continuous parameter input, while the individual-level constraint effectively bounds the entropy of its output, providing an effective solution for preserving privacy in HDVs' car-following model. Third, we systematically analyze the impact of the proposed parameter privacy filters on control performance, considering the trade-off between privacy and control performance, including fuel consumption, velocity errors, and head-to-tail string stability of the mixed-autonomy platoon. We show that the proposed parameter privacy filters can protect privacy with an acceptable impact on these performance indicators.

The rest of this paper is organized as follows. Section 2 introduces the system modeling and controller design for mixed-autonomy traffic. Section 3 presents the parameter privacy filter for mixed traffic to protect the car-following parameters. Section 4 provides the details of the learning-based estimator with individual-level privacy preservation constraints. Section 5 analyses the privacy-utility trade-off under two types of controllers. The head-to-tail string stability analysis is conducted in Section 6. Section 7 concludes the paper and proposes future research directions.

2. Mixed Traffic Modeling and Controller Design

In this section, we introduce the modeling and controller design of mixed-autonomy platoon control. Section 2.1 introduces system modeling for mixed-autonomy traffic. Section 2.2 provides the details of the CAV controller design.

2.1. System Modeling

As illustrated in Fig. 1, we consider a mixed-autonomy platoon comprising HDVs and CAVs, whereby the longitudinal actions of HDVs are characterized by the output of car-following models, and the actions

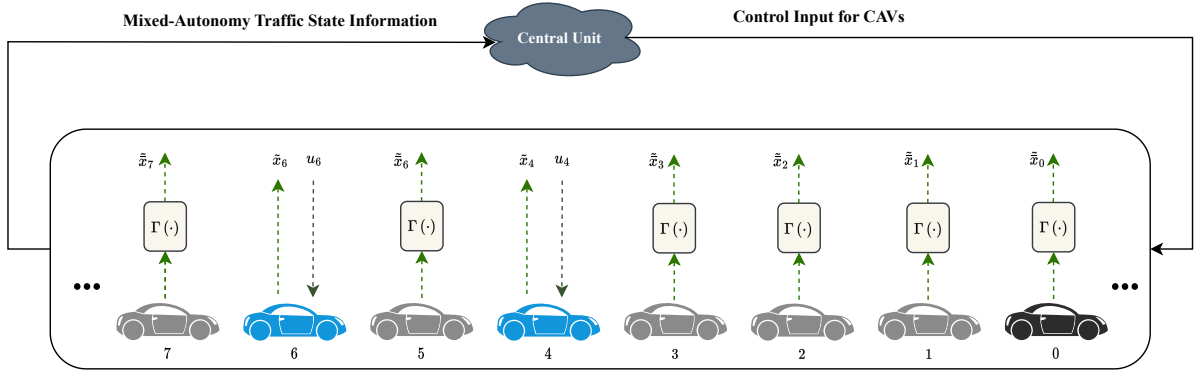


Figure 1: The figure provides an overview of a mixed traffic flow, where blue vehicles represent CAVs, gray vehicles represent HDVs, and the black vehicle denotes the head vehicle. All HDVs (except the head vehicle) are equipped with a privacy filter $\Gamma_i, i \in \Omega_H$ to protect privacy. This filter enables the central unit to receive the pseudo-states of HDVs instead of their true states, ensuring that sensitive information is not disclosed.

of CAVs are determined by a designed controller that relies on the transmitted state information from surrounding HDVs and other CAVs.

Mathematically, we consider a mixed-autonomy platoon of vehicles indexed by $i \in \Omega$ where Ω is an ordered set. Let Ω_C and Ω_H , respectively, denote the sets of CAVs and HDVs within a mixed-autonomy platoon such that $\Omega = \Omega_C \cup \Omega_H$ and $\Omega_C \cap \Omega_H = \emptyset$. For each vehicle $i \in \Omega$, we characterize its vehicle dynamics by tracking its real-time state $x_i(t) = [s_i(t), v_i(t)]^T$, where $v_i(t)$ denotes its real-time velocity, and $s_i(t)$ denotes the real-time spacing between vehicle i and its preceding vehicle $i - 1$.

Specifically, the vehicle dynamics of HDV $i \in \Omega_H$ can be written as

$$\begin{cases} \dot{s}_i(t) = v_{i-1}(t) - v_i(t), \\ \dot{v}_i(t) = \mathbb{F}_{\kappa_i}(s_i(t), v_i(t), v_{i-1}(t)), \end{cases} \quad i \in \Omega_H, \quad (1)$$

where the function $\mathbb{F}_{\kappa_i}(\cdot)$ represents the car-following model of HDV i parametrized by a vector of sensitive parameters $\kappa_i = [\omega_{i,1}, \omega_{i,2}, \dots, \omega_{i,r}]$, with $r \in \mathbb{N}^+$ indicating the number of sensitive parameters. Notice that \mathbb{F}_{κ_i} can represent any parametric car-following models that calculate HDV i 's acceleration rate $\dot{v}_i(t)$ using the spacing $s_i(t)$ between vehicle $i - 1$ and vehicle i , the velocity of vehicle i , $v_i(t)$, and the velocity of the preceding vehicle $v_{i-1}(t)$.

Similarly, the vehicle dynamics of CAV $i \in \Omega_C$ can be written as

$$\begin{cases} \dot{s}_i(t) = v_{i-1}(t) - v_i(t), \\ \dot{v}_i(t) = u_i(t), \end{cases} \quad i \in \Omega_C, \quad (2)$$

where the acceleration rate of CAV i is determined by the control action $u_i(t)$.

We can summarize Eq. (1) and Eq. (2) as a control affine system

$$\dot{x}(t) = f(x(t), v_0(t)) + Bu(t), \quad (3)$$

where $x(t) = \{x_i(t)\}_{i \in \Omega_C \cup \Omega_H} \in \mathbb{R}_+^{2n}$ and $u(t) = \{u_i(t)\}_{i \in \Omega_C} \in \mathbb{R}_+^m$ represents the states of all vehicles in the platoon and control inputs of all CAVs, respectively. Here, $n = |\Omega_C \cup \Omega_H|$ and $m = |\Omega_C|$ denote the number of vehicles and the number of CAVs, respectively. $v_0(t)$ is the velocity of the head vehicle, and $f(\cdot)$ represents the nonlinear dynamics of HDVs and the linear dynamics of CAVs. System matrix B for CAVs'

control input is given as $B = [e_{2n}^{2i_1}, e_{2n}^{2i_2}, \dots, e_{2n}^{2i_m}] \in \mathbb{R}^{2n \times m}$, where the vector $e_{2n}^i \in \mathbb{R}_+^{2n}$ associated with CAV $i \in \Omega_C$ is a vector with the $2i$ -th entry being one and the others being zeros.

In the LCC context, the central unit determines the control action $u_i(t)$ for each CAV $i \in \Omega_C$ based on the error state information transmitted from all vehicles within the platoon. Here, the error state of vehicle $j \in \Omega_C \cup \Omega_H$ is defined as $x_j^{\text{err}} = [s_j - s_j^*, v_j - v^*]$, where $x_j^* = [s_j^*, v^*]$ represents the equilibrium state of the platoon, with v^* being specified by the head vehicle and s_j^* calculated by vehicle j by solving $\mathbb{F}_{\kappa_j}(s_j^*, v^*, v^*) = 0$ from its car-following model. We represent the error state information received by the CAV from all surrounding vehicles as $y(t) = \left\{ \{\bar{x}_j^{\text{err}}(t)\}_{j \in \Omega_H}, \{x_j^{\text{err}}(t)\}_{j \in \Omega_C} \right\}$. Notice that for HDV j , here we distinguish the true error state $x_j^{\text{err}}(t)$ and the transmitted error state $\bar{x}_j^{\text{err}}(t)$ because we allow HDVs to perturb their state information from $x_j(t)$ to $\bar{x}_j(t)$ before sharing it with others to protect the privacy of their driving behavior. The perturbed state is determined by a parameter privacy filter, as presented in Section 3.

2.2. Controller Design

In our study, we employ two distinct types of controllers for the CAVs: a centralized data-driven controller and a distributed linear feedback controller. The former serves as an example of data-driven control methodologies, while the latter stands as a paradigm for distributed control systems, with the added benefit of facilitating easier string stability analysis in Section 6.

The centralized data-driven controller we use is based on the data-enabled predictive control (DeePC), as detailed in Coulson et al. (2019) and applied to mixed-autonomy platoons in Wang et al. (2023a). As DeePC works in the discrete-time linear system, we thus discretize and linearize the original system dynamics in Eq. (3) into a discrete-time linear time-invariant (LTI) system with time step denoted by t_s , for which the details are given in Appendix A.

DeePC offers a nonparametric approach that circumvents the need for system identification by directly designing control inputs using pre-collected trajectory data, the details of which are outlined in Appendix B. This pre-collected data sequence includes the control input u^d , the head vehicle's velocity error ϵ^d , and the output state y^d over a duration of $T_{\text{ini}} + N$, which is segmented into corresponding "past data" (i.e., U_p, E_p , and Y_p) of length T_{ini} and corresponding "future data" (i.e., U_f, E_f , and Y_f) of length N . Using the online collected data (i.e., $u_{\text{ini}}, \epsilon_{\text{ini}}$, and y_{ini}) of length T_{ini} and past data, DeePC calculates the non-parametric system dynamics represented by g . The future trajectory of the control input u , velocity error ϵ , and output state y is determined using the dynamics g and future data matrices U_f, E_f, Y_f . The formulation of DeePC at the t_c -th time step is given as:

$$\min_{g, u, y, \sigma_y} \sum_{t_s=t_c}^{t_c+N-1} \left(\|y(t_s)\|_Q^2 + \|u(t_s)\|_R^2 \right) + \lambda_g \|g\|_2^2 + \lambda_y \|\sigma_y\|_2^2 \quad (4)$$

$$\text{subject to } \begin{bmatrix} U_p \\ E_p \\ Y_p \\ U_f \\ E_f \\ Y_f \end{bmatrix} g = \begin{bmatrix} u_{\text{ini}} \\ \epsilon_{\text{ini}} \\ y_{\text{ini}} \\ u \\ \epsilon \\ y \end{bmatrix} + \begin{bmatrix} 0 \\ 0 \\ \sigma_y \\ 0 \\ 0 \\ 0 \end{bmatrix}, \quad (5)$$

$$\epsilon = \mathbb{O}_N, \quad (6)$$

$$s_{\min} - s^* \leq \mathbb{1}_N \otimes [\mathbb{O}_{m \times n} \quad \mathbb{1}_m] y \leq s_{\max} - s^* \quad (7)$$

$$a_{\min} \leq u \leq a_{\max}, \quad (8)$$

where the first term in the objective function penalizes the deviation from the equilibrium state weighted by matrix $Q = \text{diag}(w_v \mathbb{1}_n, w_s \mathbb{1}_n)$, with w_v and w_s indicating the penalty coefficients for velocity and spacing errors, respectively, and $\mathbb{1}_n$ represents an n -dimensional identity matrix. Similarly, the second term in the objective function seeks to penalize the energy of the control inputs, weighted by matrix $R = \text{diag}(w_u \mathbb{1}_m)$ with coefficient w_u . The third term is introduced to limit the ‘‘complexity’’ of the data-driven behavior model to prevent overfitting, while the last term ensures the feasibility of the optimization problem by relaxing the constraints. The coefficients λ_g and λ_y are positive coefficients that tune the importance of these terms. Eq. (5) represents the nonparametric model of the mixed-autonomy platoon. Eq. (6) indicates that the head vehicle aims to preserve a constant equilibrium velocity in the future. Constraint (7) provides lower and upper bounds for the future spacing between the CAV and its preceding vehicle, denoted by s_{\min} and s_{\max} , respectively. This is to prevent collisions and dampen traffic disruptions. Finally, constraint (8) enforces the actuation limits for each CAV, bounded by the minimum and maximum acceleration values a_{\min} and a_{\max} .

Regarding the distributed linear controller, we implement a strategy similar to that described in Wang et al. (2021) for CAV $i \in \Omega_C$. This strategy leverages the transmitted error states to stabilize the mixed-autonomy platoon; that is, it aims to maintain an equilibrium state (s_i^*, v^*) :

$$u_i(t) = \sum_{j_{\text{CAV}} \in \Omega_C} \left(\mu_{i,j_{\text{CAV}}} s_{j_{\text{CAV}}}^{\text{err}}(t) + \eta_{i,j_{\text{CAV}}} v_{j_{\text{CAV}}}^{\text{err}}(t) \right) + \sum_{j_{\text{HDV}} \in \Omega_H} \left(\mu_{i,j_{\text{HDV}}} \bar{s}_{j_{\text{HDV}}}^{\text{err}}(t) + \eta_{i,j_{\text{HDV}}} \bar{v}_{j_{\text{HDV}}}^{\text{err}}(t) \right), \quad (9)$$

where $\mu_{i,j_{\text{CAV}}}$, $\eta_{i,j_{\text{CAV}}}$ are the feedback gains corresponding to the states of CAVs $j_{\text{CAV}} \in \Omega_C$, and $\mu_{i,j_{\text{HDV}}}$, $\eta_{i,j_{\text{HDV}}}$ are the feedback gains corresponding to the surrounding HDVs $j_{\text{HDV}} \in \Omega_H$, which are chosen based on the string stability conditions following Wang et al. (2021).

3. Privacy Filter Design for Mixed-Autonomy Platoon

This section introduces the parameter privacy filter for LCC to protect the privacy of sensitive car-following parameters of HDVs, i.e., the parameters κ_i , against adversaries. Section 3.1 describes the assumptions and the framework of the parameter privacy filter. Section 3.2 presents the details of the randomizer, which is responsible for generating pseudo sensitive parameters based on the true sensitive parameters. Section 3.3 introduces the nonlinear transformation employed to utilize these pseudo sensitive parameters in synthesizing pseudo states.

3.1. Assumptions and Methodological Framework

Before describing the details of the parameter privacy filter in the LCC context, we present the following assumptions regarding the car-following parameters and adversaries. We first make the following two assumptions regarding the sensitive car-following parameters of HDVs.

Assumption 1 (Car-following parameters). *We assume that each HDV knows its own car-following parameters in each traffic scenario (e.g., highway, urban materials, residential areas, etc.).*

Assumption 1 is realistic as an HDV can learn its own parameters from its historical states $x_i(t)$ via any system identification methods. Note that we allow such parameters for each HDV to vary across traffic scenarios (e.g., highway, urban materials, residential areas, etc.).

Furthermore, given a population of drivers, their car-following parameters in any given scenario can be characterized by a continuous probability distribution. We make the following assumption about such a distribution.

Assumption 2 (Distribution of car-following parameters). *We assume the car-following parameter κ follows an independent and identical continuous probability distribution over a set \mathcal{K} with a probability density function $P_{\kappa}(\cdot)$, which is publicly known.*

Assumption 2 is realistic since the car-following parameter of each individual driver is her own characteristics and hence independent of other drivers. Furthermore, we assume the distribution of such parameters to be publicly known for two reasons. First, one can always learn such a prior distribution from public naturalistic vehicle trajectory datasets such as the NGSIM dataset (Punzo et al., 2011), pNEUMA dataset (Barmounakis and Geroliminis, 2020), and Waymo dataset (Ettinger et al., 2021; Chen et al., 2023). Second, this is a conservative assumption because the knowledge of such a distribution can make it easier for attackers to learn the drivers' car-following parameters, and therefore, this assumption enables us to design a stronger privacy-preserving strategy.

We then make the following assumption for adversaries who are interested in learning the sensitive parameters of HDVs.

Assumption 3 (Adversaries). *Adversaries include any external attackers who can access the data transmitted from an HDV to the central unit (e.g., by wiretapping the communication channel or attacking the database of the central unit). They aim to estimate the car-following parameters of an HDV using the following information: (1) transmitted states of all vehicles within the platoon, represented by $y(t) = \{\bar{x}_i^{err}\}_{i \in \Omega_H} \cup \{x_j^{err}\}_{j \in \Omega_C}$, and (2) the prior distribution of car-following model parameters characterized by $\phi_\kappa(\cdot)$. Specifically, adversaries can leverage any parameter estimation model to learn car-following parameters $\kappa_i = [\omega_{i1}, \omega_{i2}, \dots, \omega_{ir}]$ for HDV $i \in \Omega_H$ that minimizes the estimation performance metric of normalized mean square error (MSE), i.e., $E \left[\sum_{l=1}^r \left(\frac{\hat{\omega}_{il} - \omega_{il}}{\omega_{il}} \right)^2 \right]$.*

We make the following remarks regarding Assumption 3. First, as presented in the previous section, the central unit can access and store the transmitted error states from each HDV and then send the control command to each CAV. Hence, external attackers can attack the central units' communication channels or databases to illegally access these transmitted states and use them to infer the true parameters of each HDV via a parameter estimator. Second, certain CAVs are admittedly equipped with sensors capable of capturing the real states of surrounding vehicles, which may be potentially employed to infer sensitive parameters of surrounding vehicles. However, in practice, an HDV is typically in the sensing range of the CAV for a relatively short period of time, and therefore, the data collected about the HDV involves only short-term trajectories for particular scenarios, which can be insufficient for accurate and holistic estimation of HDV behavior. Hence, we argue that the primary privacy concerns of HDV drivers about such a system lie in the sharing of their long-term and comprehensive trajectory data to the central unit rather than the unavoidable detection of surrounding CAVs. Third, we use normalized MSE as the attacker's metric, which is simply the MSE divided by the variance of the true data. It is preferred over regular MSE because it provides a more standardized way to assess the model's performance, especially when dealing with data from different scales and magnitudes. This choice aligns well with our scenario, where κ encompasses multiple sensitive parameters with different scales, making normalized MSE a more suitable evaluation metric.

With these assumptions, we next present the parameter privacy filter, a randomized mechanism denoted by $\Gamma_i(\cdot)$ that protects sensitive parameters κ_i by generating pseudo-states \bar{x}_i from (i) true states x_i , (ii) true car-following parameters κ_i , and (iii) external inputs (i.e., the speed of the proceeding vehicle v_{i-1}). Specifically, the privacy filter for vehicle $i \in \Omega_H$ can be written as

$$\bar{x}_i = \Gamma_i(x_i, v_{i-1}, \kappa_i), i \in \Omega_H. \quad (10)$$

Let variables $X_i = \{x_i^{t_s}\}_{t_s=1}^T$ and $\bar{X}_i = \{\bar{x}_i^{t_s}\}_{t_s=1}^T$, respectively, represent a sequence of true states and pseudo states for HDV i . Here, we use the bolded variables κ and \bar{X}_i to represent the sensitive parameters and pseudo states as random variables, as described in Assumption 2 and Eq. (10), and κ and \bar{X}_i to represent

their specific realizations. We can model the general process of generating pseudo states in Eq. (10) as the following optimization problem:

$$\min_{\bar{X}_i} \mathbb{E}_{\bar{X}_i} D(X_i, \bar{X}_i) \quad (11)$$

$$\text{s.t. } I[\kappa; \bar{X}_i] \leq I_0, \quad (12)$$

where the objective function (11) minimizes the expected discrepancy between the true states and pseudo states. Constraint (12) provides an upper bound I_0 for the mutual information between true parameter κ and pseudo states \bar{X}_i to limit information leakage. A large value of $I[\cdot]$ results in a higher risk of information leakage of true sensitive parameters, while a small value of $I[\cdot]$ can ensure a higher privacy level. Here, for continuous values of κ and \bar{X}_i , the mutual information is represented as follows (\int can be changed to \sum for discrete variables):

$$I[\kappa; \bar{X}_i] = \int_{\kappa, \bar{X}_i} P(\bar{X}_i, \kappa) \log \frac{P(\bar{X}_i, \kappa)}{P(\bar{X}_i)P(\kappa)} d\kappa d\bar{X}_i. \quad (13)$$

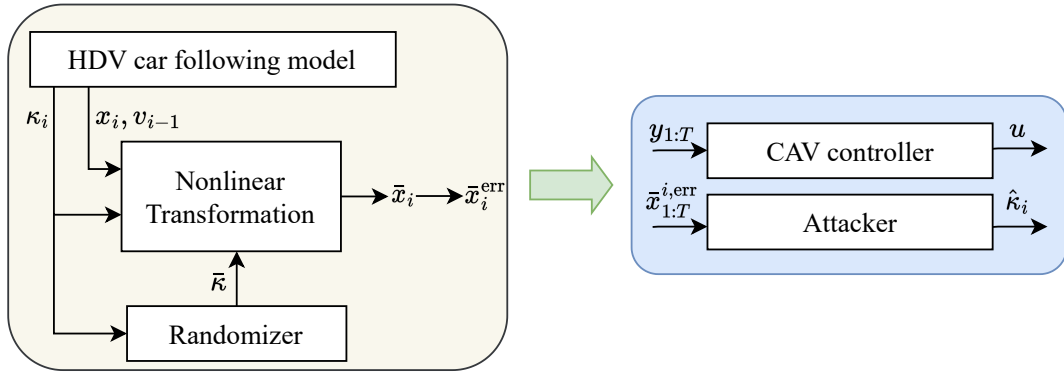


Figure 2: The structure of the privacy filter for mixed-autonomy platoon.

The optimization problem Eq. (11)-Eq. (12) is challenging to solve because the calculation of mutual information $I[\kappa; \bar{X}_i]$ is inherently difficult due to the high dimension of \bar{X}_i . Hence, we follow a heuristic approach proposed in Nekouei et al. (2022) that solves the optimization problem in a two-step manner. As illustrated in Fig. 2, the privacy filter consists of two components: (i) a randomizer that distorts the true sensitive parameters κ_i to generate pseudo parameters $\bar{\kappa}_i$ according to a probabilistic mapping $\pi(\bar{\kappa}_i|\kappa_i)$, and (ii) a nonlinear transformation that produces pseudo states \bar{x}_i from the pseudo parameters $\bar{\kappa}_i$, true states x_i , and the velocity of the preceding vehicle v_{i-1} , such that adversaries cannot infer the true parameters from the pseudo error states.

Remark 1. In this paper, although we do not explicitly design a parameter privacy filter for CAVs, the devised privacy filter can also be applied in a similar manner to protect the privacy of the control gains of CAVs, which can be seen as a trade secret of the car manufacturer. Moreover, we demonstrate that CAV parameter privacy can be preserved by applying the privacy filter for the vehicle ahead due to the interconnected structure of the platoon system. For example, as in Fig. 1, HDV 3 is equipped with a privacy filter, while there is no privacy preservation for CAV 4. Consequently, the inference attacker receives the pseudo velocity \bar{v}_3^{err} rather than the true velocity v_3^{err} . This can substantially impact any inference attacks for the CAV 4 even though it is not equipped with a privacy filter because the preceding vehicle's velocity is crucial for estimating the control gain or car-following parameter of the following vehicle.

Next, we present the details of the two steps in Section 3.2 and Section 3.3 and extend the approach in Section 4.

3.2. Randomizer

The randomizer generates a pseudo parameter $\bar{\kappa} \in \bar{\mathcal{K}}$ using the true parameter $\kappa \in \mathcal{K}$ according to a probabilistic mapping $\pi(\bar{\kappa} | \kappa)$. Let us first follow the original assumption made for the randomizer proposed in Nekouei et al. (2022), which requires both the set of true parameters, i.e., \mathcal{K} , and the set of pseudo parameters, i.e., $\bar{\mathcal{K}}$, to be discrete sets. Such an assumption is made without loss of generality, as one can always discretize the continuous parameter space into multiple subsets, with the mean value of each subset being selected as its representative value used in the discrete parameter space. Note that for pseudo parameters, these subsets are specified by HDVs to better protect privacy and simplify the derivation of the filter. Such an assumption will be relaxed to consider the continuous true parameter set \mathcal{K} in Section 4, whereby we devise a neural network-based approximator to find close-to-optimal probabilistic mappings for each true parameter in the continuous parameter space.

Now, we present the mathematical formulation of the randomizer following Nekouei et al. (2022). Let us discretize the considered time horizon into T time intervals indexed by t_s , each with size T_{step} . The probabilistic mapping $\pi(\bar{\kappa} | \kappa)$ can be found via the following optimization problem.

$$\min_{\{\pi(\bar{\kappa}|\kappa)\}_{\bar{\kappa} \in \bar{\mathcal{K}}, \kappa \in \mathcal{K}}} \frac{1}{T} \sum_{t_s=1}^T \mathbb{E} \left[\left\| x_i^{t_s} - \bar{x}_i^{t_s} \right\|^2 \right] \quad (14)$$

$$\text{s.t. } \pi(\bar{\kappa} | \kappa) \geq 0, \quad \forall \kappa \in \mathcal{K}, \forall \bar{\kappa} \in \bar{\mathcal{K}}, \quad (15)$$

$$\sum_{\bar{\kappa} \in \bar{\mathcal{K}}} \pi(\bar{\kappa} | \kappa) = 1, \quad \forall \kappa \in \mathcal{K}, \quad (16)$$

$$\mathbf{I}[\boldsymbol{\kappa}; \bar{\boldsymbol{\kappa}}] \leq I_0, \quad (17)$$

where the bolded variable $\boldsymbol{\kappa}$ and $\bar{\boldsymbol{\kappa}}$ represent the true and pseudo parameters as random variables. The variable $\left\{ x_i^{t_s} \right\}_{t_s=1}^T$ represents a sampled trajectory (i.e., sequence of states) generated from the true parameters $\boldsymbol{\kappa}$ at discretized time steps indexed by t_s , and $\left\{ \bar{x}_i^{t_s} \right\}_{t_s=1}^T$ sampled trajectory generated from the distorted parameters $\bar{\boldsymbol{\kappa}}$ at discretized time steps indexed by t_s , both using Monte Carlo sampling. The objective function Eq. (14) minimizes the expected errors in the reported measurement due to the parameter distortion of the privacy filter, which can be calculated by:

$$\begin{aligned} \frac{1}{T} \sum_{t_s=1}^T \mathbb{E} \left[\left\| x_i^{t_s} - \bar{x}_i^{t_s} \right\|^2 \right] &= \sum_{\kappa \in \mathcal{K}} \sum_{\bar{\kappa} \in \bar{\mathcal{K}}} \frac{1}{T} \sum_{t_s=1}^T \mathbb{E} \left[\left\| x_i^{t_s} - \bar{x}_i^{t_s} \right\|^2 \middle| \boldsymbol{\kappa} = \kappa, \bar{\boldsymbol{\kappa}} = \bar{\kappa} \right] \Pr(\boldsymbol{\kappa} = \kappa, \bar{\boldsymbol{\kappa}} = \bar{\kappa}) \\ &= \sum_{\kappa \in \mathcal{K}} \sum_{\bar{\kappa} \in \bar{\mathcal{K}}} \frac{1}{T} \sum_{k=1}^T \mathbb{E} \left[\left\| x_i^{t_s} - \bar{x}_i^{t_s} \right\|^2 \middle| \boldsymbol{\kappa} = \kappa, \bar{\boldsymbol{\kappa}} = \bar{\kappa} \right] \Pr(\bar{\boldsymbol{\kappa}} = \bar{\kappa} | \boldsymbol{\kappa} = \kappa) \Pr(\boldsymbol{\kappa} = \kappa) \\ &= \sum_{\kappa \in \mathcal{K}} \sum_{\bar{\kappa} \in \bar{\mathcal{K}}} e(\kappa, \bar{\kappa}) \pi(\bar{\kappa} | \kappa) P_{\boldsymbol{\kappa}}(\kappa), \end{aligned} \quad (18)$$

where recall that $P_{\boldsymbol{\kappa}}(\cdot)$ represents the prior distribution for the car-following parameter $\boldsymbol{\kappa}$ among the entire driver population, which is assumed as public knowledge (as in Assumption 2). Variable $e(\kappa, \bar{\kappa})$ denotes the trajectory distortion between true and pseudo vehicle states $\left\{ x_i^{t_s} \right\}_{t_s=1}^T$ and $\left\{ \bar{x}_i^{t_s} \right\}_{t_s=1}^T$, generated respectively

with parameters κ and $\bar{\kappa}$:

$$e(\kappa, \bar{\kappa}) = \frac{1}{T} \sum_{t_s=1}^T \mathbb{E} \left[\left\| x_i^{t_s} - \bar{x}_i^{t_s} \right\|^2 \middle| \kappa = \kappa, \bar{\kappa} = \bar{\kappa} \right], \quad (19)$$

which can be obtained via Monte Carlo sampling and can be seen as a constant. Note that $P_{\kappa}(\kappa)$ is known *a priori*. Hence the objective function written as Eq. (18) is a linear function of the decision variables $\{\pi(\bar{\kappa} | \kappa)\}_{\kappa \in \mathcal{K}, \bar{\kappa} \in \bar{\mathcal{K}}}$.

Constraints Eq.(15) and Eq.(16) ensure that the probabilistic mapping $\pi(\cdot | \cdot)$ is a probabilistic distribution. Constraint Eq.(17) provides an upper bound I_0 for the mutual information between κ and $\bar{\kappa}$, defined as

$$\begin{aligned} I[\kappa; \bar{\kappa}] &= \sum_{\kappa \in \mathcal{D}, \bar{\kappa} \in \bar{\mathcal{K}}} \Pr(\kappa = \kappa, \bar{\kappa} = \bar{\kappa}) \log \frac{\Pr(\kappa = \kappa, \bar{\kappa} = \bar{\kappa})}{\Pr(\kappa = \kappa) \Pr(\bar{\kappa} = \bar{\kappa})} \\ &= \sum_{\kappa \in \mathcal{D}, \bar{\kappa} \in \bar{\mathcal{K}}} \pi(\bar{\kappa} | \kappa) P_{\kappa}(\kappa) \log \frac{\pi(\bar{\kappa} | \kappa)}{\sum_{\kappa' \in \mathcal{D}} \pi(\bar{\kappa} | \kappa') P_{\kappa}(\kappa')}, \end{aligned} \quad (20)$$

where mutual information $I[\cdot]$ between the true gains and the pseudo gains indicates the amount of information about κ that can be inferred from $\bar{\kappa}$. Meanwhile, by Nekouei et al. (2021), the mutual information between the true gains κ and the shared information $\bar{\mathbf{x}}_{1:T}$ can be upper bounded by the mutual information between the true and pseudo gains, i.e., $I[\kappa; \bar{\mathbf{x}}_{1:T}] \leq I[\kappa; \bar{\kappa}]$, which, together with the privacy preservation constraint in Eq. (17), implies $I[\kappa; \bar{\mathbf{x}}_{1:T}] \leq I_0$, i.e., the output of the privacy filter provides an upper-bounded level of information about the car-following parameters κ . In fact, according to Theorem 3 in Nekouei et al. (2022), with the mutual information upper-bound I_0 , the error probability of any parameter estimator used by the adversaries can be lower bounded, i.e.,

$$\Pr(\kappa \neq \hat{\kappa}(\bar{\mathbf{x}}_i^{1:T}, \mathbf{v}_{i-1}^{1:T})) \geq \frac{H[\kappa] - I_0 - 1}{\log |\mathcal{D}|}, \quad (21)$$

where $|\mathcal{K}|$ is the cardinality of \mathcal{K} , and $H[\kappa]$ is the discrete entropy of κ . It is evident that the lower bound of $\Pr(\kappa \neq \hat{\kappa}(\bar{\mathbf{x}}_i^{1:T}, \mathbf{v}_{i-1}^{1:T}))$ increases as I_0 decreases, which means a small I_0 can reduce the chance that an attacker reliably estimates the car-following parameters.

The optimization problem Eq. (14) - Eq. (17) is a convex optimization problem since both the objective and constraints Eq. (15)-Eq. (16) are linear and the mutual information at the left-hand side of Eq. (17) is convex. Note that if the number of subsets becomes too large (e.g., κ has a high dimension), finding the probabilistic mapping can still become intractable due to the extensive computational resources required for Monte Carlo sampling and a significantly large number of decision variables. To accelerate the computation, we will devise a learning-based approach to interpolate the probabilistic mapping with a neural network, which facilitates better generalization of the method to continuous parameter space. Details for the learning-based acceleration will be described in Section 4.

With the derived probabilistic mapping $\pi(\bar{\kappa} | \kappa)$, we next introduce the nonlinear transformation that converts $\pi(\bar{\kappa} | \kappa)$ to pseudo states that will be transmitted to CAVs.

3.3. Nonlinear Transformation

The nonlinear transformation module is a synthetic data generator that leverages the pseudo parameters to generate pseudo states $\bar{\mathbf{x}}$ such that the joint probabilistic distribution function (p.d.f.) of $\bar{\mathbf{x}}$ is ‘‘convincing’’. Specifically, let $\kappa = [\omega_1, \omega_2, \dots, \omega_r]$ denote the true parameters of car-following model, and let $\bar{\kappa} = [\bar{\omega}_1, \bar{\omega}_2, \dots, \bar{\omega}_r]$ denote the pseudo parameters chosen by the randomizer. The p.d.f. of the true states is

represented by $p_\kappa(x_{1:T})$ parametrized by κ . What we mean by ‘‘convincing’’ is that after the nonlinear transformation, the p.d.f. of pseudo states is $p_{\bar{\kappa}}(\bar{x}_{1:T})$ parametrized by $\bar{\kappa}$. In other words, we want to joint distribution of the pseudo states to be consistent with the assumed pseudo parameter $\bar{\kappa}$.

Recall that the number of vehicles in the platoon is n and the number of CAVs is m , and hence, we have a total of $n - m$ privacy filters $\{\Gamma_i\}_{i \in \Omega_{\mathcal{H}}}$. Then, in the t_s -th step of the simulation, with $i \in \Omega_{\mathcal{C}}, j \in \Omega_{\mathcal{H}}$, the output of the filter $\{\Gamma_i\}_{i \in \mathcal{H}}$ for HDVs is

$$\bar{x}_{k,\mathcal{H}} = \left[\bar{s}_{j_1}(t_s), \bar{v}_{j_1}(t_s), \dots, \bar{s}_{j_{n-m}}(t_s), \bar{v}_{j_{n-m}}(t_s) \right]^\top, \quad (22)$$

where only the states of HDVs are transformed because the proposed privacy filter is designed to protect HDVs’ car-following parameters. The states of the CAV can be represented as:

$$x_{t_s,\mathcal{C}} = \left[s_{i_1}(t_s), v_{i_1}(t_s), \dots, s_{i_m}(t_s), v_{i_m}(t_s) \right]^\top. \quad (23)$$

After nonlinear transformation, the measurement output at t_s -step for the CAVs is $y_{t_s} = \left[\bar{x}_{t_s,\mathcal{H}}; x_{t_s,\mathcal{C}} \right]$.

Using the sets of true gains $\{\kappa_j\}_{j \in \Omega_{\mathcal{H}}}$ and pseudo gains $\{\bar{\kappa}_j\}_{j \in \Omega_{\mathcal{H}}}$, we generate pseudo states using a recursive scheme by a total number of $n - m$ privacy filters according to:

$$\Gamma_{j_1} \rightarrow \begin{cases} \bar{v}_{j_1}(t_s) = F_{\bar{v}_{j_1}}^{-1} \left(d_1(t_s) \mid \bar{s}_{j_1}(t_s - 1), \bar{v}_{j_1}(t_s - 1), v_0(t_s - 1), \bar{\kappa}_1 \right), \\ d_1(t_s) = F_{v_{j_1}} \left(v_{j_1}(t_s) \mid s_{j_1}(t_s - 1), v_{j_1}(t_s - 1), v_0(t_s - 1), \kappa_1 \right), \\ \bar{s}_{j_1}(t_s) = F_{\bar{s}_{j_1}}^{-1} \left(d_2(t_s) \mid \bar{s}_{j_1}(t_s - 1), \bar{v}_{j_1}(t_s - 1), \bar{v}_{j_1}(t_s), v_0(t_s - 1), \bar{\kappa}_1 \right), \\ d_2(t_s) = F_{s_{j_1}} \left(s_{j_1}(t_s) \mid s_{j_1}(t_s - 1), v_{j_1}(t_s - 1), v_{j_1}(t_s), v_0(t_s - 1), \kappa_1 \right), \\ \dots \end{cases} \quad (24)$$

$$\Gamma_{j_{n-m}} \rightarrow \begin{cases} \bar{v}_{j_{n-m}}(t_s) = F_{\bar{v}_{j_{n-m}}}^{-1} \left(d_{2(n-m)-1}(t_s) \mid \bar{s}_{j_{n-m}}(t_s - 1), \bar{v}_{j_{n-m}}(t_s - 1), v_{j_{n-m-1}}(t_s - 1), \bar{\kappa}_{n-m} \right), \\ d_{2(n-m)-1}(t_s) = F_{v_{j_{n-m}}} \left(v_{j_{n-m}}(t_s) \mid s_{j_{n-m}}(t_s - 1), v_{j_{n-m}}(t_s - 1), v_{j_{n-m-1}}(t_s - 1), \kappa_{n-m} \right), \\ \bar{s}_{j_{n-m}}(t_s) = F_{\bar{s}_{j_{n-m}}}^{-1} \left(d_{2(n-m)}(t_s) \mid \bar{s}_{j_{n-m}}(t_s - 1), \bar{v}_{j_{n-m}}(t_s - 1), \bar{v}_{j_{n-m}}(t_s), v_{j_{n-m-1}}(t_s - 1), \bar{\kappa}_{n-m} \right), \\ d_{2(n-m)}(t_s) = F_{s_{j_{n-m}}} \left(s_{j_{n-m}}(t_s) \mid s_{j_{n-m}}(t_s - 1), v_{j_{n-m}}(t_s - 1), v_{j_{n-m}}(t_s), v_{j_{n-m-1}}(t_s - 1), \kappa_{n-m} \right), \end{cases} \quad (25)$$

where v_0 is the velocity of the head vehicle, and F denotes the conditional cumulative distribution function (c.d.f.), i.e., $F_v(z \mid v_n, x_n, \kappa) = \int_{-\infty}^z p_{\kappa,v}(z \mid v_n, x_n) dz$. The velocity of the preceding vehicle is recognized as an external input of the system. The structure of the nonlinear transformation utilizes a feedforward-feedback scheme. The feedforward part computes the conditional c.d.f. $d_1, \dots, d_{2(n-m)}$, while the feedback part computes the pseudo states $\bar{s}_{j_1}, \bar{v}_{j_1}, \dots, \bar{s}_{j_{n-m}}, \bar{v}_{j_{n-m}}$ using the output of the privacy filter.

4. Learning-Based Acceleration for Randomizer with Continuous Parameter Space

In this section, we introduce a learning-based approach for accelerating the solution process of the randomizer to facilitate the online deployment of the parameter privacy filter. Recall that in Section 3, we handle continuous true car-following parameters by discretizing them into multiple subsets and then

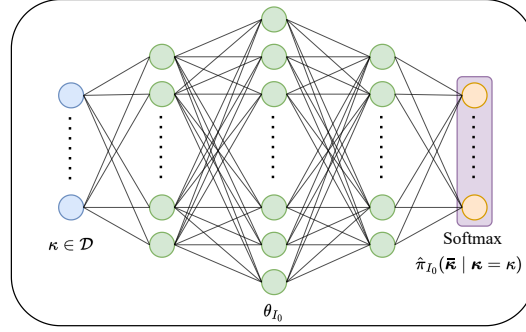


Figure 3: Neural Network-based Randomizer Structure.

solve a convex optimization to determine a probabilistic mapping that distorts the true parameters into pseudo parameters. However, if the number of subsets becomes too large (e.g., scenarios with high parameter dimensions or high requirements of discretization resolution), solving the convex optimization problem can become intractable due to a large number of decision variables, especially with the Monte-Carlo sampling required to calculate the error $e(\kappa, \bar{\kappa})$. The proposed learning-based approach can address this challenge by designing a neural network with few training samples and using it to interpolate the probabilistic mapping $\pi(\bar{\kappa}|\kappa)$ over a continuous parameter space $\kappa \in \mathcal{K}$.

Moreover, within the trained neural network, we further strengthen the privacy guarantee. Note that constraint Eq. (17) provides an upper bound for the amount of information leaked by sharing the pseudo states \bar{X} , which works in an aggregated manner over all parameters in \mathcal{K} without imposing privacy guarantee for any specific parameter. Therefore, it is likely that privacy is not well guaranteed for certain parameters, especially those that appear in \mathcal{K} with a low probability, leading to fairness issues among drivers. To address this issue, we will strengthen constraint Eq. (17) by providing a guarantee for each individual parameter $\kappa \in \mathcal{K}$ and then integrate the strengthened constraint into the neural network.

In the rest of this section, we present first the learning-based acceleration approach in Section 4.1 and then the strengthened privacy preservation constraints in Section 4.2.

4.1. Neural Network-Based Randomizer

Similar to the randomizer for discrete parameter space, we can formulate the following optimization problem in scenarios with continuous true sensitive parameters:

$$\min_{\pi(\bar{\kappa}|\kappa)} \int_{\kappa \in \mathcal{K}} \sum_{\bar{\kappa} \in \bar{\mathcal{K}}} \pi(\bar{\kappa} | \kappa) P_{\kappa}(\kappa) e(\kappa, \bar{\kappa}) d\kappa \quad (26)$$

$$\text{s.t. } \sum_{\bar{\kappa} \in \bar{\mathcal{K}}} \pi(\bar{\kappa} | \kappa) = 1, \forall \kappa \in \mathcal{K}, \quad (27)$$

$$I[\bar{\kappa}; \kappa] \leq I_0, \quad (28)$$

$$\pi(\bar{\kappa} | \kappa) \geq 0, \forall \kappa \in \mathcal{K}, \bar{\kappa} \in \bar{\mathcal{K}}, \quad (29)$$

with

$$e(\kappa, \bar{\kappa}) = \frac{1}{T} \sum_{t_s=1}^T \mathbb{E} \left[\left\| x_i^{t_s} - \bar{x}_i^{t_s} \right\|^2 \middle| \kappa = \kappa, \bar{\kappa} = \bar{\kappa} \right], \quad (30)$$

$$I[\kappa; \bar{\kappa}] = \int_{\kappa \in \mathcal{K}} \sum_{\bar{\kappa} \in \bar{\mathcal{K}}} \pi(\bar{\kappa} | \kappa) P_{\kappa}(\kappa) \log \frac{\pi(\bar{\kappa} | \kappa)}{\int_{\kappa' \in \mathcal{K}} \pi(\bar{\kappa} | \kappa') P_{\kappa}(\kappa') d\kappa'} d\kappa, \quad (31)$$

where the key difference compared to Eq. (14)-(17) lies in replacing the summation over a discrete set \mathcal{D} with the integration over a continuous set \mathcal{K} . Recall that $P_{\kappa}(\kappa)$ is the probability density function for κ . The optimization problem over the continuous parameter space can be challenging to solve due to its functional form. Note that it is more desirable if the set of pseudo states is discrete because this can help reduce computation complexity and better protect parameter privacy.

As depicted in Fig. 3, to efficiently solve the optimization problem Eq (26) - Eq (29), we design a neural network-based estimator $h_{\theta_{I_0}}(\kappa)$, $\kappa \in \mathcal{K}$ parameterized by θ_{I_0} to approximate the probabilistic mapping. The last layer of the neural network is configured as a softmax function to ensure that the output vector conforms to a probabilistic distribution, where each element corresponds to a possible pseudo parameter $\bar{\kappa} \in \bar{\mathcal{K}}$. Such a neural network can be used to estimate the probability distribution $\hat{\pi}_{I_0}(\bar{\kappa} | \kappa = \kappa) = h_{\theta_{I_0}}(\kappa)$ for any given $\kappa \in \mathcal{K}$.

We then describe the training procedure for such a neural network-based estimator.

Training dataset. We collect the training dataset using the randomizer with discrete parameter space. Similar to the previous section, we discretize the continuous parameter set into multiple subsets, which could follow certain rules (e.g., grids) or stochastic sampling. We select the representative value of each subset as its mean value and solve the optimization problem Eq. (14)-Eq. (17) with these representative values denoted by set \mathcal{D} to obtain the corresponding probabilistic mapping $\pi(\cdot)$ with each privacy level I_0 . Then, the set of $\{(\kappa, \pi(\bar{\kappa}|\kappa))\}_{\kappa \in \mathcal{D}}$ is used as the training dataset. We can further repeat the aforementioned procedure several times to randomly generate multiple discretized parameter sets \mathcal{D} and combine the resulting training datasets.

Loss function. Since our objective is to match the output distribution $\hat{\pi}_{I_0}(\bar{\kappa} | \kappa = \kappa)$ to a given distribution $\pi_{I_0}(\bar{\kappa} | \kappa = \kappa)$, we employ the Kullback-Leibler (KL) divergence (Van Erven and Harremos, 2014) as the loss function. The KL divergence is utilized to measure the distance between two distributions and is given by:

$$D_{\text{KL}}\left(\hat{\pi}_{I_0}(\bar{\kappa} | \kappa = \kappa) \parallel \pi_{I_0}(\bar{\kappa} | \kappa = \kappa)\right) = \sum_{\bar{\kappa} \in \bar{\mathcal{K}}} \sum_{\kappa \in \mathcal{D}} \hat{\pi}_{I_0}(\bar{\kappa} = \bar{\kappa} | \kappa = \kappa) \log \left(\frac{\hat{\pi}_{I_0}(\bar{\kappa} = \bar{\kappa} | \kappa = \kappa)}{\pi_{I_0}(\bar{\kappa} = \bar{\kappa} | \kappa = \kappa)} \right). \quad (32)$$

With the designed neural network, we can approximate the optimal probabilistic mapping of the randomizer in scenarios with continuous parameter space. However, the constraint Eq. (17) is not guaranteed to be satisfied. Moreover, Eq. (17) only imposes a privacy guarantee at an aggregated level, not for each specific true car-following parameter. We will explicitly incorporate the individual-level privacy preservation constraint into the neural network in the next subsection.

4.2. Individual-Level Privacy Preservation Constraint

In this subsection, we integrate an individual-level privacy guarantee into the neural network. Specifically, we will strengthen the constraint Eq. (17).

By the properties of mutual information and conditional entropy, we can write the mutual information between κ and $\bar{\kappa}$ as:

$$I[\kappa; \bar{\kappa}] = H(\bar{\kappa}) - H(\bar{\kappa} | \kappa) = H(\bar{\kappa}) - \int_{\kappa \in \mathcal{K}} P_{\kappa}(\kappa = \kappa) H(\bar{\kappa} | \kappa = \kappa) d\kappa, \quad (33)$$

where $H(\bar{\kappa})$ represents the entropy of random variable $\bar{\kappa}$, i.e., $H(\bar{\kappa}) = -\sum_{\bar{\kappa} \in \bar{\mathcal{K}}} P_{\bar{\kappa}}(\bar{\kappa} = \bar{\kappa}) \log(P_{\bar{\kappa}}(\bar{\kappa} = \bar{\kappa}))$, and $H(\bar{\kappa} | \kappa)$ represents the entropy of $\bar{\kappa}$ conditional on κ .

Hence, we can rewrite Eq. (33) as

$$\int_{\kappa \in \mathcal{K}} f_{\kappa}(\kappa = \kappa) H(\bar{\kappa} | \kappa = \kappa) d\kappa = -I[\kappa; \bar{\kappa}] + H(\bar{\kappa}) \geq -I_0 + H(\bar{\kappa}), \quad (34)$$

where the last inequality is derived by integrating Eq. (17).

Note that Eq. (34) is an aggregated-level constraint that aggregates over all parameters $\kappa \in \mathcal{K}$ and hence provides no guarantee for the privacy level of any specific parameter. To address this issue, we strengthen the inequality and provide a more robust constraint for the neural network-based randomizer. Specifically, we require that for any specific parameter κ , the conditional entropy $H(\bar{\kappa} | \kappa = \kappa)$ satisfies:

$$H(\bar{\kappa} | \kappa = \kappa) \geq -I_0 + H(\bar{\kappa}). \quad (35)$$

As the entropy of $\bar{\kappa}$, i.e., $H(\bar{\kappa})$, can be estimated using Monte Carlo simulation with the original neural network-based randomizer and I_0 is a positive constant, the right side of the inequality is also a constant for every $\kappa = \kappa$. Consequently, we define inequality Eq. (35) as the individual-level privacy preservation constraint, which guarantees a specific bound on the conditional entropy for any given $\kappa = \kappa$.

To integrate the inequality constraint Eq. (35) into the neural network, we modify the softmax layer of the neural network. Assume the values of the neural network's output layer are $m_1, m_2, \dots, m_n \in \mathbb{R}$, where n is the number of random variables for the output probabilistic mapping.

Then we define the output of the softmax layer for element $i \in \{1, \dots, n\}$ as:

$$\hat{\pi}_{I_0}(\bar{\kappa} = \bar{\kappa}^i | \kappa = \kappa) = \frac{e^{\frac{m_i}{T_{\text{scale}}}}}{\sum_{i=1}^n e^{\frac{m_i}{T_{\text{scale}}}}}, \quad (36)$$

where T_{scale} denotes the designed scaling factor, and its value directly impacts the entropy of the output probabilistic mapping. Adjusting T_{scale} , we can effectively fine-tune the output entropy. Consequently, we integrate Eq. (36) to the individual-level privacy preservation constraint:

$$-\sum_{i=1}^n \hat{\pi}_{I_0}(\bar{\kappa} = \bar{\kappa}^i | \kappa = \kappa) \log \hat{\pi}_{I_0}(\bar{\kappa} = \bar{\kappa}^i | \kappa = \kappa) \geq -I_0 + H(\bar{\kappa}). \quad (37)$$

We set $T_{\text{scale}} = 1$ initially. Then, if Eq. (37) does not hold, we find a suitable T_{scale} by solving $-\sum_{i=1}^n \frac{e^{\frac{m_i}{T_{\text{scale}}}}}{\sum_{i=1}^n e^{\frac{m_i}{T_{\text{scale}}}} \log \frac{e^{\frac{m_i}{T_{\text{scale}}}}}{\sum_{i=1}^n e^{\frac{m_i}{T_{\text{scale}}}}} = -I_0 + H(\bar{\kappa})$, so that the modified probabilistic mapping Eq. (36) with scaling factor T_{scale} satisfies the individual-level privacy preservation constraint. Note that during the training process, T_{scale} is set to a fixed value of 1, and the constraint becomes active only during offline testing.

With the neural-network-based randomizer and individual-level privacy preservation constraint introduced above, we have a comprehensive framework for the continuous parameter privacy filter. In Section 5 and Section 6, we will evaluate the effectiveness of this approach within the context of a mixed-autonomy platoon.

5. Analysis of Privacy-Utility Trade-Off

This section presents numerical analyses to demonstrate the privacy-utility trade-off of the proposed framework. Section 5.1 describes the simulation setting. Section 5.2 performs privacy analysis for HDVs in different mixed-autonomy platoon scenarios as shown in Fig. 4, whereby adversaries aim to infer the sensitive parameters of HDVs from the reported state information. Section 5.3 quantifies the impact of the privacy filter on the CAV controller in terms of fuel consumption and average absolute velocity error.

5.1. Simulation Setting

In this paper, following the setting of LCC (Wang et al., 2021), we use the optimal velocity model (OVM) (Bando et al., 1998) for the HDVs' car-following model as an example:

$$\ddot{V}(\cdot) = \alpha_i (V(s_i(t)) - v_i(t)) + \beta_i (v_{i-1}(t) - v_i(t)), \quad (38)$$

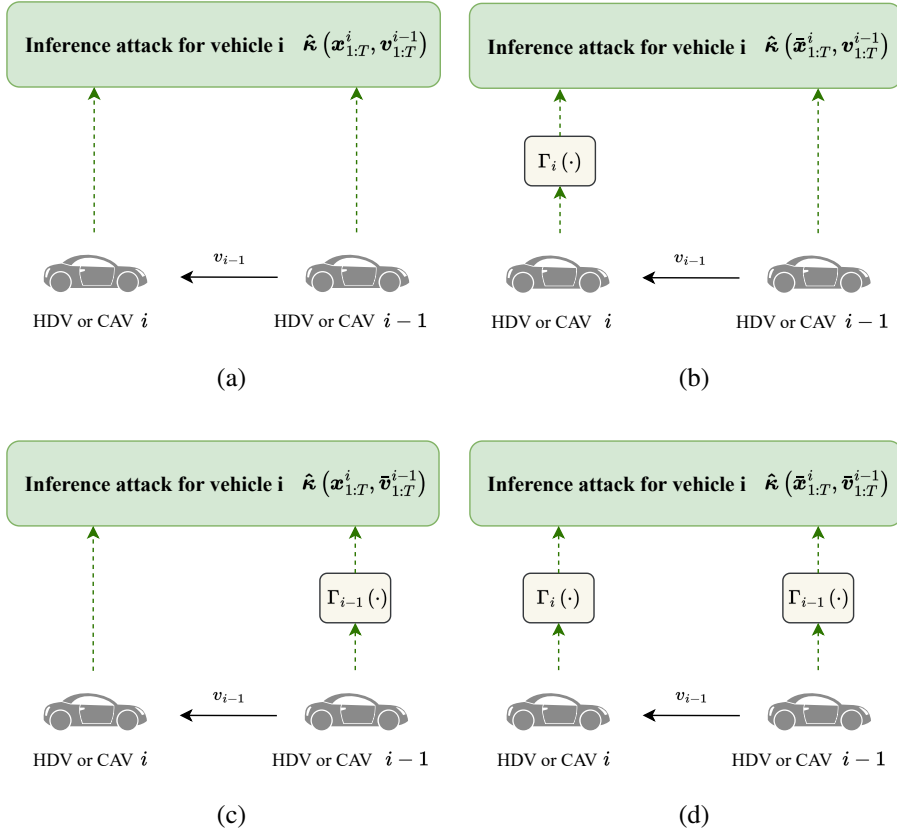


Figure 4: Different scenarios for parameter privacy-preserving platooning control. (a) is the scenario that the vehicle i does not have any privacy preservation. For scenarios (b - d), the parameter privacy for vehicle i is preserved at different levels.

where α_i and β_i are positive constants for HDV $i \in \Omega_H$ representing sensitivity coefficients, $V(s)$ represents the spacing-dependent desired velocity of human drivers with a specific form indicated below:

$$V(s) = \begin{cases} 0, & s \leq s_{st} \\ g_v(s), & s_{st} < s < s_{go} \\ v_{max}, & s \geq s_{go} \end{cases} \quad (39)$$

where s_{st} and s_{go} represent two spacing thresholds, and v_{max} represents the maximum velocity. For simplicity of comparison, we assume that s_{st} , s_{go} , and v_{max} are identical for each vehicle. Between the two thresholds s_{st} and s_{go} , the desired velocity $V(s)$ can be written as a function of spacing $g_v(s)$:

$$g_v(s) = \frac{v_{max}}{2} \left(1 - \cos \left(\pi \frac{s - s_{st}}{s_{go} - s_{st}} \right) \right). \quad (40)$$

Note that the attacker is not interested in learning s_{st} and s_{go} because the driving behavior (e.g., aggressiveness) is more intuitively reflected by gains α , β . In other words, the sensitive parameter for HDV i can be presented as $\kappa_i = [\alpha_i, \beta_i]$. The parameter setting for the experiments is shown in Table 1.

Table 1

Parameters setup

Parameters	s_{st}	s_{go}	a_{min}	a_{max}	$\mu_{2,0}$	$\eta_{2,0}$	$\mu_{2,1}$	$\eta_{2,1}$	$\mu_{2,2}$
Values	5	35	-5	5	0	0.05	-0.05	0.3	0.2
Parameters	$\eta_{2,2}$	$\mu_{2,3}$	$\eta_{2,3}$	$\mu_{2,4}$	$\eta_{2,4}$	$\mu_{2,5}$	$\eta_{2,5}$	$\mu_{2,6}$	$\eta_{2,6}$
Values	-0.6	-0.1	0.15	-0.05	0.1	-0.01	0.08	-0.01	0.05
Parameters	v^*	s^*	T_{step}	T_{ini}	w_v	w_s	w_u	λ_g	λ_y
Values	15	20	0.01	0.2	1	0.5	0.1	1	1e3

5.2. Performance of Privacy Preservation

In this subsection, we evaluate the privacy protection performance of the parameter privacy filter. Specifically, we consider a scenario as shown in Fig. 1 where an adversary with the shared error states attempts to infer the sensitive parameters of HDV 2. The head vehicle aims to maintain a specific target speed but has a sine-like velocity disturbance with an amplitude of 3 m/s. The central unit receives the reported error state information from HDV 2 and attempts to estimate its car-following parameters. The car-following parameters of HDV 2 is $\kappa = [0.6, 0.9]$.

We investigate different implementation scenarios of the parameter privacy filter, as shown in Fig. 4. The scenario in Fig. 4 (a) represents a baseline where neither the preceding nor the ego vehicle employs a privacy filter, leaving the HDV parameters exposed and unshielded. In contrast, the scenario shown in Fig. 4 (b) illustrates the case where the ego vehicle utilizes a privacy filter, actively safeguarding its own parameter privacy. The scenario shown in Fig.4 (c) evaluates the effect of equipping the preceding vehicle with a privacy filter, which, due to the system's interconnectivity, inadvertently enhances the parameter privacy of the ego vehicle as well. The scenario shown in Fig.4 (d) presents a scenario where both the preceding and the ego vehicles are equipped with privacy filters.

We employ an attacker model to quantify the level of privacy protection in these scenarios. The attackers in the simulation (i.e., any adversary who can access the transmitted data of an HDV to the central unit) are assumed to use the non-linear least squares method (Teunissen, 1990) to estimate the sensitive parameters of HDVs from the reported error states. We use this method because it is a classic and effective approach for nonlinear system identification. Note that since HDVs report a sequence of distorted error states instead of distorted raw states, the attacker needs to simultaneously estimate the sensitive parameter κ_i and the equilibrium state s_i^* . To this end, the attacker can add a constraint to the attacker model, i.e., $\mathbb{F}_{\kappa_i}(s_i^*, v^*, v^*) = 0$, whereby the equilibrium velocity v^* can be easily obtained from the head vehicle. Specifically, for OVM, this constraint can be represented by $s_i^* = \frac{s_{go} - s_{st}}{\pi} \arccos\left(1 - \frac{2v^*}{v_{max}}\right) + s_{st} \forall i \in \Omega_H$.

With the attacker model, we characterize the privacy protection performance by the attackers' estimation accuracy of the sensitive parameters, i.e., normalized MSE. We evaluate such a performance index in the aforementioned privacy scenarios by comparing the following three methods with various levels of privacy considerations: (1) the parameter privacy filter with various levels of I_0 , and (2) a noise-adding mechanism with additive Gaussian random noise, an approach to enhance privacy by introducing stochasticity to the original state sequence (as has been done in the existing literature), and (3) no privacy considerations. The comparison between these three methods demonstrates the value of the parameter privacy filter in protecting sensitive parameters in car-following models.

Our evaluation encompasses the parameter privacy performance of both the original discrete parameter privacy filter in Section 5.2.1 and our proposed continuous parameter privacy approach in Section 5.2.2.

5.2.1. Discrete Parameter Privacy Filter for HDVs

We first present the results in discrete parameter space to show the effectiveness of the canonical parameter privacy filter as proposed in Section 3. Here, the true gains for the 5 HDVs take values in the following set with equal probability:

$$\mathcal{K} = \left\{ \begin{bmatrix} 0.6 \\ 0.9 \end{bmatrix}, \begin{bmatrix} 0.5 \\ 0.95 \end{bmatrix}, \begin{bmatrix} 0.65 \\ 0.85 \end{bmatrix}, \begin{bmatrix} 0.6 \\ 0.8 \end{bmatrix}, \begin{bmatrix} 0.65 \\ 0.9 \end{bmatrix} \right\}.$$

The pseudo sensitive parameters are selected from the following set by solving the randomizer Eq. (14) - Eq. (17):

$$\bar{D} = \left\{ \begin{bmatrix} 0.5 \\ 0.8 \end{bmatrix}, \begin{bmatrix} 0.2 \\ 0.4 \end{bmatrix} \right\}.$$

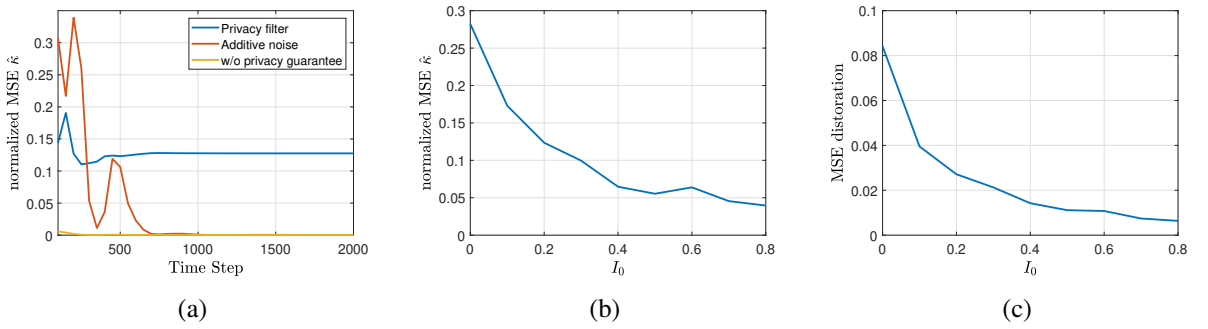


Figure 5: Simulation results for the scenario in Fig. 4 (b) using discrete parameter privacy filter. (a) normalized MSE of the gain estimator as a function of time when $I_0 = 0.2$, the intensity of the Gaussian additive noise is 0.2. (b) The normalized MSE error of the gain estimator versus the level of information leakage I_0 . (c) Average total distortion versus the level of information leakage I_0 .

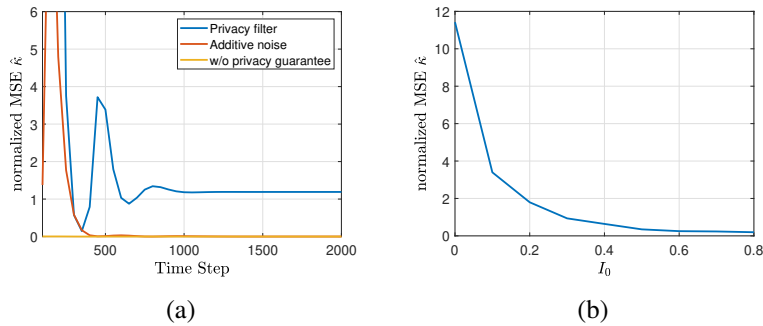


Figure 6: Simulation results for the scenario in Fig. 4 (c) using discrete parameter privacy filter. (a) normalized MSE of the gain estimator as a function of time when $I_0 = 0.2$, the intensity of the Gaussian additive noise is 0.2. (b) The normalized MSE error of the gain estimator versus the level of information leakage I_0 .

Fig. 5, Fig. 6 and Fig. 7 show the simulation results to evaluate the performance of privacy protection of the three scenarios as illustrated in Fig. 4 (b)-Fig. 4 (d), respectively. Overall, the results demonstrate that the parameter privacy filter consistently performs effectively in all three scenarios, with the trade-off between privacy and utility being influenced by the selected privacy level I_0 .

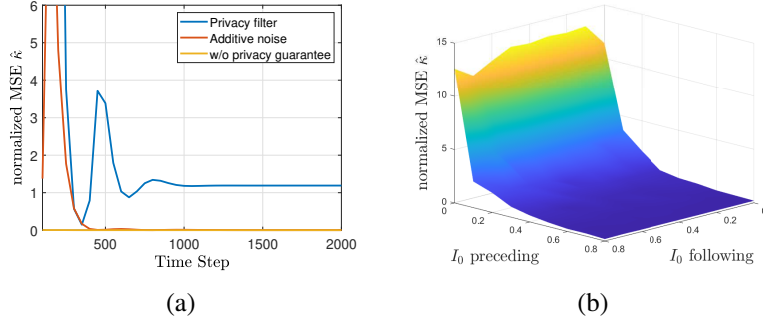


Figure 7: Simulation results for the scenario in Fig. 4 (d) using discrete parameter privacy filter. (a) normalized MSE of the gain estimator as a function of time when I_0 preceding = 0.2 and I_0 following = 0.2, the intensity of the Gaussian additive noise is 0.2. (b) x-axis and y-axis represent the privacy level I_0 for the preceding and following vehicle, the z-axis denotes the normalized MSE error of the gain estimator.

Value of the parameter privacy filter. As illustrated in Fig. 5 (a), we compare the parameter estimation error of the three methods mentioned above: the parameter privacy filter, noise-adding mechanism with additive Gaussian noise, and no privacy protection. The privacy level of the privacy filter, I_0 , is set to 0.2, and the mean of the Gaussian additive noise is set to 0.2 to ensure similar distortion levels of the system states for these two methods. The results indicate that the MSE of $\hat{\kappa}$ converges after approximately 700 steps for all three methods. Furthermore, the parameter privacy filter can prevent adversaries from accurately reconstructing the sensitive parameters from the shared data, as the normalized MSE for this method converges to a relatively high value of 0.15. On the other hand, both of the other two methods fail to protect these sensitive parameters, as the adversaries can eventually accurately infer these parameters. This is expected as the noise added by the noise-adding mechanism can be easily smoothed by any filtering algorithm. This shows that the parameter privacy filter can effectively protect the sensitive parameters of HDVs' car-following models.

Impact of the privacy level I_0 . As illustrated in Fig. 5 (b) and (c), the normalized MSE of $\hat{\kappa}$ and the state distortion decreases as I_0 increases. This is because the privacy bound of the randomizer will be relaxed as I_0 increases. Note that the relation between these two values and I_0 is not strictly decreasing because the choice of $\bar{\kappa}$ is random.

Impact of implementing the parameter privacy filter on the preceding vehicle. As mentioned in Remark 1, implementing the parameter privacy filter on the preceding vehicle can help protect the parameter privacy of the ego vehicle. This conclusion can be validated by the results shown in Fig. 6, where a predetermined privacy level $I_0 = 0.2$ is used. In fact, the level of protection is even better if the parameter filter is implemented in the preceding vehicle because the external input (i.e., v_{i-1}) significantly influences the estimation accuracy of the attacker. Moreover, in Fig. 7 (a), it is evident that if both the preceding and the ego vehicles implement the parameter privacy filter, the sensitive parameters of the ego vehicle can be effectively protected. In particular, it is shown in Fig. 7 (b), the effectiveness of privacy preservation is influenced by both the privacy level of the privacy filter installed in the preceding vehicle and the privacy level of the following vehicle itself.

5.2.2. Continuous Parameter Privacy Filter for HDVs

In reality, the true sensitive parameters of the car-following model are from a continuous space \mathcal{K} . To simulate this, both α and β are assumed to follow a uniform distribution over the range $[0, 1]$. The set of pseudo parameters is also uniformly selected from \mathcal{K} and can be expressed as $\bar{\mathcal{K}} = \{[\alpha_i, \beta_j]\}_{\alpha_i \in \mathcal{M}, \beta_j \in \mathcal{M}}$, where the discrete set for pseudo parameter $\mathcal{M} = \{0.1, 0.2, 0.3, 0.4, 0.5, 0.6, 0.7, 0.8, 0.9, 1\}$. For the neural

network-based randomizer, we utilized a fully connected neural network with an input size of 2, two hidden layers comprising 200 and 300 neurons, respectively, and an output layer of size 9.

With the integration of the neural network-based randomizer and the individual-level privacy preservation constraint, we have the following results for the three scenarios as illustrated in Fig. 4(b)-(d).

Value of the parameter privacy filter. The results of the three methods with different levels of privacy considerations are illustrated in Fig. 8, Fig. 9, and Fig. 10, which reveal that the privacy-preserving performance of the privacy filter aligns with that of the discrete version. These results effectively demonstrate the efficacy of the proposed neural network-based randomizer and the individual-level privacy preservation constraints.

Value of individual privacy preservation constraints. To demonstrate the value of considering individual privacy preservation constraints, we compare the entropy of the output distribution corresponding to the respective sensitive parameters resulting from two parameter privacy filters: (1) the one with aggregated privacy preservation constraints (no individual-level consideration) and (2) the one with individual privacy preservation constraints. The results are shown in Fig. 11. Comparing Fig. 11(a), Fig. 11(b), and Fig. 11(c) to Fig. 11(d), Fig. 11(e), and Fig. 11(f), respectively, we can see that the individual-level privacy preservation constraints in Fig. 11(d), Fig. 11(e), and Fig. 11(f) enhance the privacy protection of all individual values of the sensitive parameter κ .

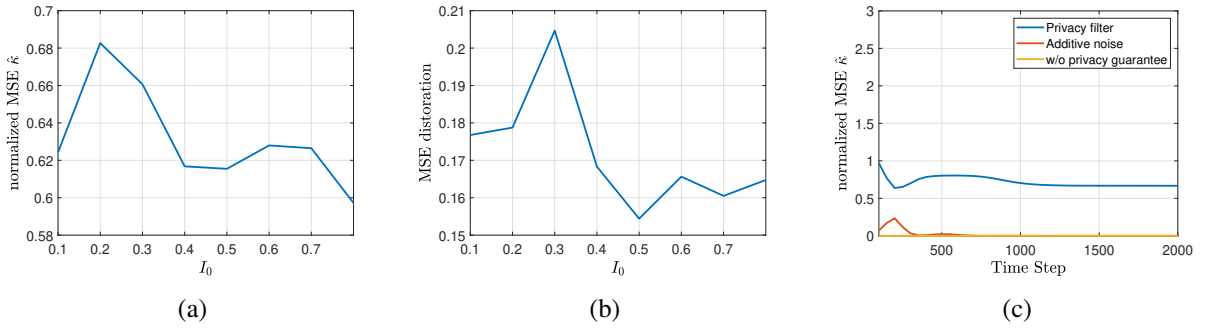


Figure 8: Simulation results for the scenario in Fig. 4 (b) using continuous parameter privacy filter. (a) The normalized MSE error of the gain estimator versus the level of information leakage I_0 . (b) Average total distortion versus the level of information leakage I_0 . (c) normalized MSE of the gain estimator as a function of time when $I_0 = 0.2$, the intensity of the Gaussian additive noise is 0.2.

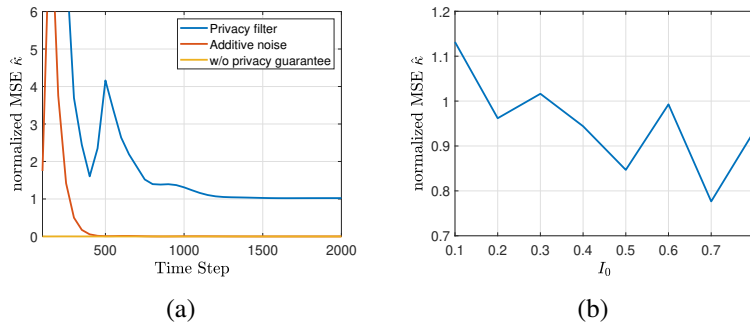


Figure 9: Simulation results for the scenario in Fig. 4 (c) using continuous parameter privacy filter. (a) normalized MSE of the gain estimator as a function of time when $I_0 = 0.2$, the intensity of the Gaussian additive noise is 0.2. (b) The normalized MSE error of the gain estimator versus the level of information leakage I_0 .

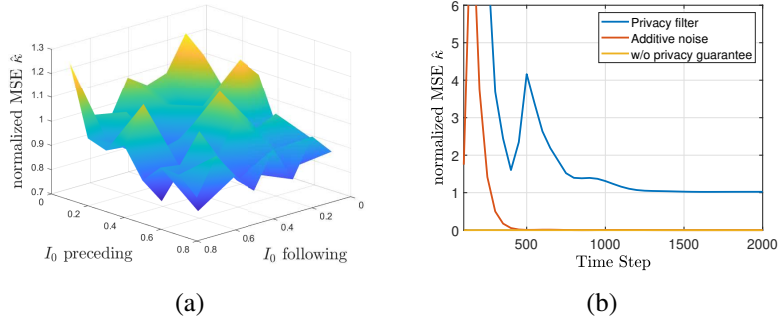


Figure 10: Simulation results for the scenario in Fig. 4 (d) using continuous parameter privacy filter. (a) normalized MSE of the gain estimator as a function of time when I_0 preceding = 0.2 and I_0 following = 0.2, the intensity of the Gaussian additive noise is 0.2. (b) x-axis and y-axis represent the privacy level I_0 for the preceding and following vehicle, the z-axis denotes the normalized MSE error of the gain estimator.

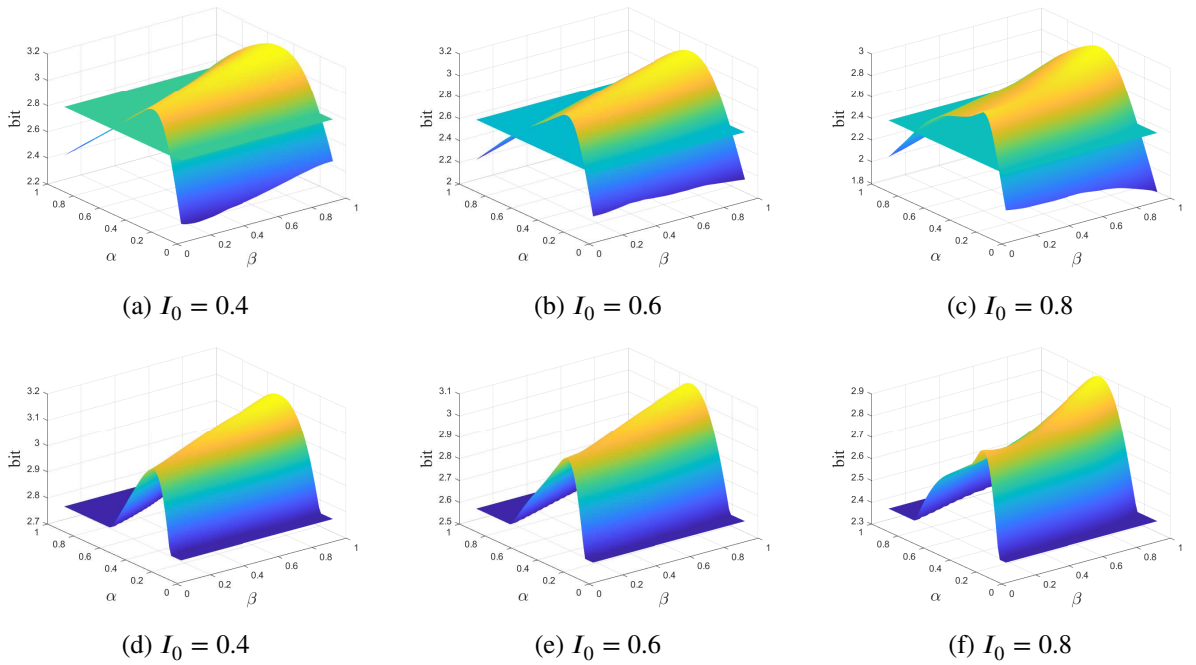


Figure 11: Continuous privacy filters using neural network-based randomizer for HDVs with different privacy levels I_0 . The x-axis and y-axis represent different sensitive parameters, while the z-axis depicts the entropy of the output distribution corresponding to the respective sensitive parameters. (a), (b) and (c) demonstrate the results without individual-level privacy preservation constraints, where the green plane is the entropy bound of the individual-level privacy preservation constraint. (d), (e) and (f) are the results with individual-level privacy preservation constraints.

5.3. Impact on the CAV Controller

To evaluate the impact of the continuous parameter privacy filter on the CAV controller for mixed-autonomy platoons, we consider a scenario with 5 HDVs with indices $\Omega_H = \{1, 3, 4, 5, 6\}$, 1 CAV with index $\Omega_C = \{2\}$, and 1 head vehicle with index 0. We assume that the head vehicle aims to maintain an equilibrium speed but has a sine-like velocity disturbance with an amplitude of 3m/s and the simulation time

A Parameter Privacy-Preserving Strategy for Mixed-Autonomy Platoon Control

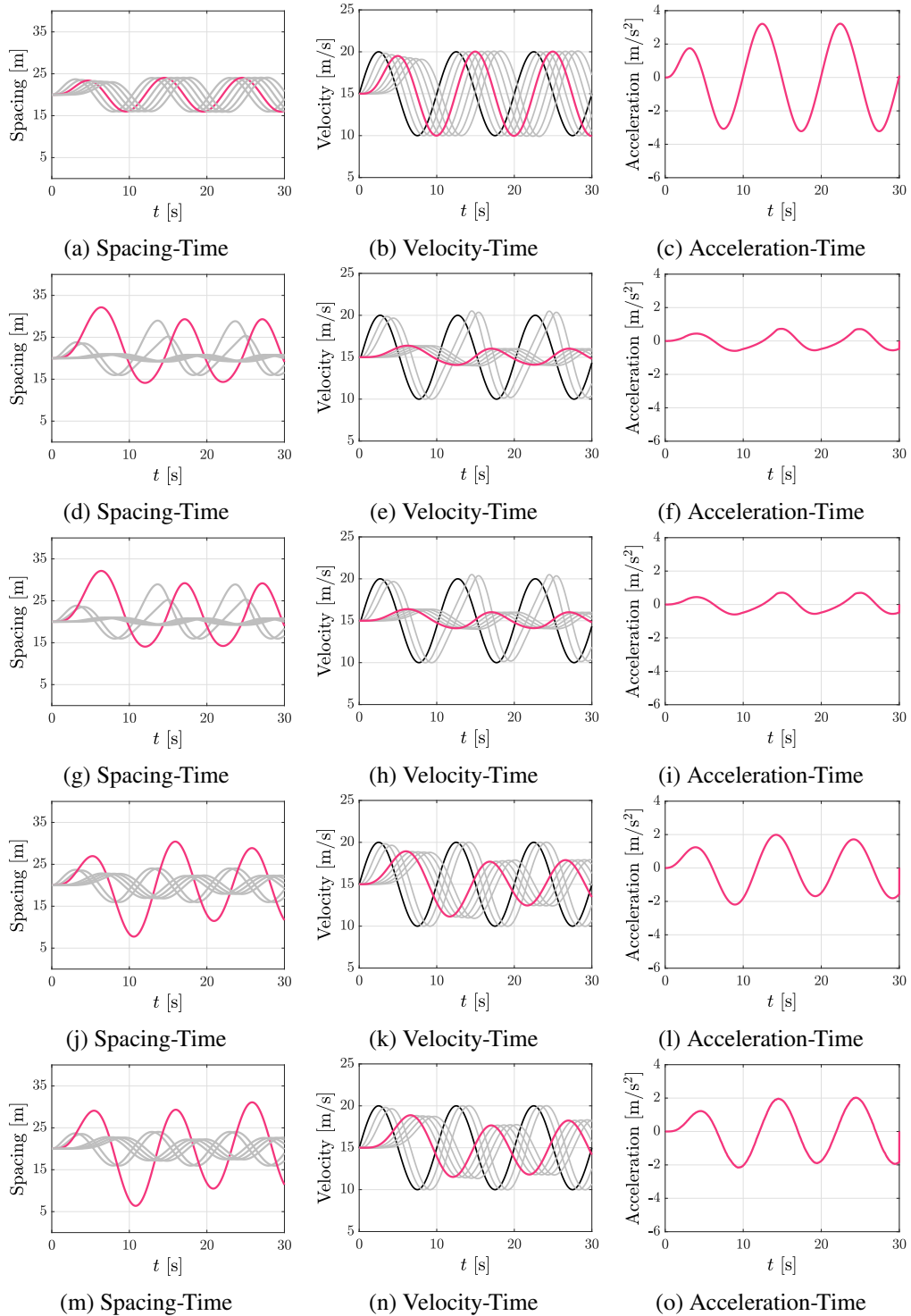


Figure 12: The simulation results for different scenarios, where subfigures (a), (b), and (c) represent the scenario without LCC, subfigures (d), (e), and (f), represent the scenario with LCC utilizing the DeePC but without the privacy filter, subfigures (g)(h)(i) represent the scenario with LCC utilizing the DeePC and the privacy filter, subfigures (j)(k)(l) represent the scenario with LCC utilizing the linear controller but without the privacy filter and subfigures (m)(n)(o) represent the scenario with LCC utilizing the linear controller and the privacy filter. The head vehicle is illustrated by the black line, on which a sine-like disturbance is applied. The two CAVs are illustrated by blue and red lines, respectively, and the HDVs are illustrated by grey lines.

Table 2

Fuel Consumption and Average Absolute Velocity Error (AAVE)

	Fuel Consumption [mL]	AAVE
Without LCC	690.18	0.30
LCC using DeePC w/o privacy filter	313.25	0.22
LCC using DeePC with privacy filter	312.99	0.22
LCC using linear controller w/o privacy filter	483.07	0.27
LCC using linear controller with privacy filter	496.18	0.27

is 30s. We evaluate the fuel consumption and velocity tracking errors (i.e. the relative velocity difference between the specified vehicle and the head vehicle) to quantify the traffic performance of five scenarios:

- (i) The scenario without LCC where the CAV adopts the same car-following models as HDVs, which does not require HDVs to share their data.
- (ii) The scenario with LCC where the CAV utilizes the DeePC but without the parameter privacy filter, which requires HDV data but offers no privacy protection.
- (iii) The scenario with LCC where the CAV utilizes the DeePC and the parameter privacy filter (applied to all HDVs), which requires HDV data and offers privacy protection.
- (iv) The scenario with LCC where the CAV utilizes the linear controller but without the parameter privacy filter, which requires HDV data but offers no privacy protection.
- (v) The scenario with LCC where the CAV utilizes the linear controller and the parameter privacy filter (applied to all HDVs), which requires HDV data and offers privacy protection.

The comparison of LCC performance with and without the privacy filter reveals the impact of the parameter privacy filter on the control efficacy of the CAV. Specifically, for the i -th vehicle, the fuel consumption rate (mL/s) is calculated based on an instantaneous model proposed in Bowyer et al. (1985) given by:

$$f_i = \begin{cases} 0.444 + 0.090R_i v_i + [0.054a_i^2 v_i]_{a_i > 0}, & \text{if } R_i > 0 \\ 0.444, & \text{if } R_i \leq 0 \end{cases} \quad (41)$$

with $R_i = 0.333 + 0.00108v_i^2 + 1.200a_i$. The Average Absolute Velocity Error (AAVE) is used to quantify velocity errors, which is obtained by computing the average of $\frac{|v_i(t) - v_0(t)|}{v_0(t)}$ over all vehicles and the entire simulation period.

Table 2 presents the fuel consumption and AAVE in different scenarios, and Fig. 12 illustrates the evolution of system states in different scenarios. It is observed that the adoption of the continuous parameter privacy filter will slightly influence system performance due to the generated noises for both the DeePC and linear feedback controller. However, the resulting system performance is still significantly better than the scenario without LCC, which suggests that the privacy filter does not undermine the benefits of LCC. With the privacy filter applied to LCC using DeePC, we observe a significant reduction in fuel consumption by approximately 54.6%, and the Average Absolute Velocity Error (AAVE) sees a reduction of about 26.7%. In the case of the linear controller equipped with the privacy filter, there is also a notable improvement, with fuel consumption dropping by roughly 28.11% and the AAVE decreasing by around 10%.

6. Head-To-Tail String Stability Analysis

In this section, we perform an analysis of the trade-off between privacy and head-to-tail string stability (Jin and Orosz, 2014) when implementing the parameter privacy filter. If the platoon has a poor head-to-tail string stability performance (Swaroop and Hedrick, 1996), stop-and-go patterns may emerge in the traffic flow, leading to a significant surge in travel time, fuel consumption, and the potential for accidents. While head-to-tail string stability has been investigated in the LCC (Wang et al., 2021) to facilitate designing the linear feedback controller, in our scenario, the distortion of the reported states received by the CAV can substantially impact the performance of the CAV controller and hence influence the string stability of the mixed-autonomy platoon system.

To analyze the influence of different pseudo parameters on head-to-tail string stability, we first construct the head-to-tail transfer function for the studied mixed-autonomy platoon, where HDVs are implemented with privacy filters, and the CAV utilizes the linear feedback controller as in Eq. (9). Subsequently, we perform numerical analysis to obtain specific head-to-tail string stable regions of different pseudo parameters, systematically exploring the impact of different pseudo parameters on the overall string stability of the system.

6.1. Head-To-Tail Transfer Function

We first provide the concept of head-to-tail string stability. For a sequence of vehicles in a platoon, the definition of head-to-tail string stability is presented below.

Definition 1 (Head-to-Tail String Stability (Jin and Orosz, 2014)). *Given the velocity deviation for the vehicle at the head of a platoon as v_h^{err} and the one at the tail of a platoon as v_t^{err} , along with their respective Laplace transforms V_h^{err} and V_t^{err} , the head-to-tail transfer function is defined as follows:*

$$T(s) = \frac{V_t^{err}}{V_h^{err}}. \quad (42)$$

Then the system is said to be head-to-tail stable if and only if:

$$|T(j\omega)|^2 < 1, \forall \omega \geq 0. \quad (43)$$

with $j^2 = -1$.

To quantify the impact of the parameter privacy filter on the string stability, we next provide the formulation of the head-to-tail transfer function, whereby the details of the derivation are given in Appendix C.

Assume the number of preceding vehicles and following vehicles of the CAV is m and n , then we have the head-to-tail transfer function of the mixed-autonomy platoon as:

$$T(s) = G(s)K^{n+m}(s), \quad (44)$$

where $K(s)$ is the local transfer function for the HDV, $G(s)$ is the local transfer function for the CAV. The specific forms of $K(s)$ and $G(s)$ are given below.

After the Laplace transform, the local velocity transfer function for HDV i can be calculated as:

$$K(s) = \frac{V_i^{err}}{V_{i-1}^{err}} = \frac{\alpha_3 s + \alpha_1}{s^2 + \alpha_2 s + \alpha_1}, \quad (45)$$

where V_{i-1}^{err} represents the Laplace transform for the velocity deviation of vehicle $i - 1$, which serves as input to the dynamic model of HDV i , and V_i^{err} represents the Laplace transform for the velocity deviation of HDV i . The coefficients α_1 , α_2 , and α_3 represent the parameters of the linearized car-following model.

Similarly, we can also write the local transfer function between the pseudo velocity deviation of HDV i , \bar{v}_i , and the true velocity deviation of vehicle $i - 1$, v_{i-1}^{err} :

$$\bar{K}(s) = \frac{\bar{\alpha}_3 s + \bar{\alpha}_1}{s^2 + \bar{\alpha}_2 s + \bar{\alpha}_1}. \quad (46)$$

Following our derivation in Appendix C, the transfer function for the CAV, $G(s)$, can be represented by:

$$G(s) = \frac{W_2(s) + W_4(s)}{R(s) + W_1(s) + W_3(s)}, \quad (47)$$

where

$$\begin{aligned} R(s) &= \frac{s^2 - k_{i_{\text{cav}}} s - \mu_{i_{\text{cav}}}}{s}, \\ W_1(s) &= \sum_{i \in \Omega_p \setminus \bar{\Omega}_p} \left(\mu_i \frac{1 - K(s)}{s K^{i_{\text{cav}}-i}(s)} + k_i \frac{1}{K^{i_{\text{cav}}-i-1}(s)} \right), \\ W_2(s) &= \sum_{i \in \Omega_p \setminus \bar{\Omega}_p} \left(\mu_i \frac{1}{s} (1 - K(s)) K^{i-i_{\text{cav}}-1}(s) + k_i K^{i-i_{\text{cav}}}(s) \right), \\ W_3(s) &= \sum_{j \in \bar{\Omega}_p} \left(\mu_j \frac{1 - \bar{K}(s)}{s K^{i_{\text{cav}}-j}(s)} + k_j \frac{\bar{K}(s)}{K^{i_{\text{cav}}-j}(s)} \right), \\ W_4(s) &= \sum_{j \in \Omega_F} \left(\mu_j \frac{1}{s} (1 - \bar{K}(s)) K^{j-i_{\text{cav}}-1}(s) + k_j \bar{K}(s) K^{j-i_{\text{cav}}-1}(s) \right), \end{aligned}$$

with Ω_p representing the ordered set for all preceding HDVs of the CAV, $\bar{\Omega}_p$ indicating the ordered subset of Ω_p for all preceding HDVs equipped with privacy filters of the CAV, Ω_F denoting the ordered set for all following HDVs of the CAV and $\bar{\Omega}_F$ referring to the ordered subset of Ω_F for all following HDVs equipped with privacy filters of the CAV.

Moreover, for two special cases where only one preceding HDV or following HDV is equipped with a privacy filter, we have $W_4 = 0$ or $W_3 = 0$. The head-to-tail transfer function formulation of the two special cases can be given as:

$$T_1(s) = \frac{W_2(s)}{R(s) + W_1(s) + W_3(s)} K^{n+m}(s), \quad (48)$$

$$T_2(s) = \frac{W_2(s) + W_4(s)}{R(s) + W_1(s)} K^{n+m}(s). \quad (49)$$

For simplicity, we will then analyze the string stable region for the two special cases mentioned above, whereby the string stable condition is met if $|T(j\omega)| \leq 1$.

6.2. Head-To-Tail String Stable Region

For simplicity of analysis, we consider a less complex scenario where there is a mixed-autonomy platoon with five vehicles, with the 3rd vehicle being a CAV and the remaining vehicles being HDVs. Specifically, only one HDV is equipped with a privacy filter. We perform numerical simulations for four cases, each with an HDV being equipped with a privacy filter. The results for these four cases on the head-to-tail string stable regions, as defined by Eq. (48) and Eq. (49), are illustrated in Fig. 13. In this analysis, we maintain

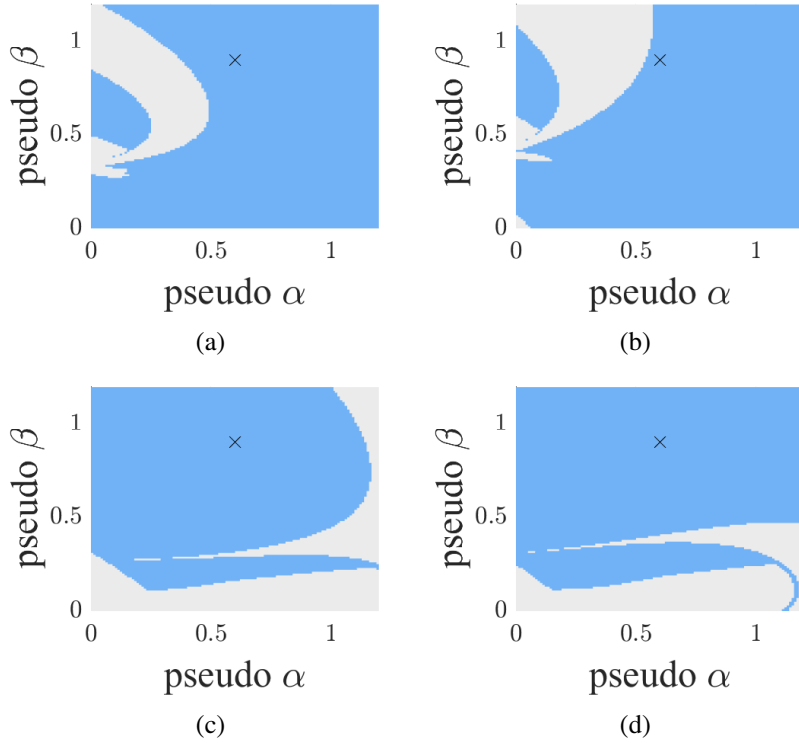


Figure 13: Head-to-tail string stable region within a platoon of 5 vehicles, with the 3rd vehicle being a CAV and the remaining vehicles being HDVs, we explore four distinct scenarios. In each case, denoted as (a), (b), (c), and (d), we investigate the string stable region for the 1-st, 2-nd, 4-th, and 5-th vehicles, respectively, each equipped with a privacy filter. The depicted blue region denotes the string stable area, while the grey region represents the string unstable area. The corresponding parameters for the position with “x” indicate the true parameters for the car-following dynamics. The x -axis and y -axis correspond to the pseudo-sensitive parameters α and β , both ranging from 0 to 1.2.

constant feedback gains and true sensitive parameters to observe variations in the string stable region under different pseudo parameters. The blue-colored regions in Fig. 13 denote the string stable regions with pseudo parameters, while the gray-colored region indicates the string unstable region attributed to the influence of pseudo parameters.

To establish a baseline, we select feedback gains that ensure traffic flow stability without a privacy filter. Specifically, the feedback gains for the CAV are set as $\mu = [0, -0.15, 0.2, -0.15, -0.1]$, and $\eta = [0.25, 0.35, -0.5, 0.35, 0.25]$. Fig. 13 (a) and (b) depict scenarios where the first HDV and the second HDV are equipped with privacy filters, respectively. Notably, the shapes of the regions are similar, but the unstable region in (b) is larger, attributed to the greater amplitude of feedback gains for the second vehicle compared to the first.

Similarly, Fig. 13 (c) and (d) showcase scenarios where the 4th HDV and 5th HDV are equipped with privacy filters, respectively. The shapes of the unstable regions are similar, while the unstable region in (d) is larger than in (c) due to the higher amplitude of feedback gains for the 4-th HDV’s state compared to the 5-th HDV.

In summary, the implementation of the devised parameter privacy filter may make originally string-stable scenarios string unstable. With fixed control gains, the shape and area of the string unstable regions are influenced by whether the HDV with a privacy filter is following or leading the CAV and the corresponding

amplitude of the state feedback gain of the HDV. Notably, in situations where multiple vehicles are positioned between the HDV with a privacy filter and the CAV, the amplitude of feedback gains for the HDV is typically small in controller design. As a result, the influence on the string unstable region remains limited and can be negligible. Additionally, by judiciously choosing particular pseudo parameters for the privacy filter, it is possible to preserve the head-to-tail string stability within the platoon.

7. Conclusions and Future Studies

This paper presents a parameter privacy filter to protect the car-following parameters of HDVs in mixed-autonomy platoon control so that adversaries cannot infer these parameters from vehicle states shared by HDVs. The proposed parameter privacy filter distorts the shared vehicle states through two components, i.e., a randomizer and a nonlinear transformation module, whereby the randomizer generates pseudo parameters from the true parameters, and the nonlinear transformation module disguises the HDV's true parameters as the pseudo parameters. In addition to the canonical version that only handles discrete vehicle states, we better tailor the parameter privacy filter to mixed-autonomy platoon control with continuous parameter space by enhancing the computation efficiency via a neural network-based randomizer. Moreover, we further strengthen privacy preservation constraints to provide privacy protection to drivers with each value of the parameter in order to enhance the reliability and practicality of the approach. Subsequently, we analyze the head-to-tail string stability of the mixed-autonomy platoon when subjected to perturbations from privacy filters. This analysis reveals that the impact of the proposed parameter privacy filter on the string stable region is acceptable. The simulation results illustrate that our approach effectively preserves parameter privacy for HDVs with marginal impact on fuel consumption and velocity deviation error. Furthermore, our results show that applying the privacy filter to the preceding vehicle can also help protect the parameter privacy of the following vehicle.

This research opens several interesting directions for future work. First, we are interested in designing a parameter privacy filter for other transportation systems with a higher dimension of parameters, such as ride-sharing systems. Second, we will extend the privacy filter to protect parameters in networked systems with arbitrary topology, such as scenarios with lane changes.

Authorship Contribution Statement

Jingyuan Zhou: Methodology, Validation, Writing - original draft. **Kaidi Yang:** Conceptualization, Methodology, Writing - original draft.

Acknowledgment

The authors would like to thank Qiqing Wang, Chaopeng Tan and Longhao Yan for fruitful discussions. This study was supported by the Singapore Ministry of Education (MOE) under its Academic Research Fund Tier 1 (A-8000404-01-00). This article solely reflects the opinions and conclusions of its authors and not Singapore MOE or any other entity.

References

- Apostolakis, T., Makridis, M.A., Kouvelas, A., Ampountolas, K., 2023. Energy-based assessment and driving behavior of acc systems and humans inside platoons. *IEEE Transactions on Intelligent Transportation Systems* .
- Bando, M., Hasebe, K., Nakanishi, K., Nakayama, A., 1998. Analysis of optimal velocity model with explicit delay. *Physical Review E* 58, 5429.
- Barmounakis, E., Geroliminis, N., 2020. On the new era of urban traffic monitoring with massive drone data: The pneuma large-scale field experiment. *Transportation research part C: emerging technologies* 111, 50–71.
- Bowyer, D.P., Akçelik, R., Biggs, D., 1985. Guide to fuel consumption analyses for urban traffic management. 32.
- Cai, S., Lyu, X., Li, X., Ban, D., Zeng, T., 2021. A trajectory released scheme for the internet of vehicles based on differential privacy. *IEEE Transactions on Intelligent Transportation Systems* 23, 16534–16547.

- Chen, C., Wang, J., Xu, Q., Wang, J., Li, K., 2021. Mixed platoon control of automated and human-driven vehicles at a signalized intersection: dynamical analysis and optimal control. *Transportation research part C: emerging technologies* 127, 103138.
- Chen, K., Ge, R., Qiu, H., Ai-Rfou, R., Qi, C.R., Zhou, X., Yang, Z., Ettinger, S., Sun, P., Leng, Z., et al., 2023. Womd-lidar: Raw sensor dataset benchmark for motion forecasting. *arXiv preprint arXiv:2304.03834*.
- Coulson, J., Lygeros, J., Dörfler, F., 2019. Data-enabled predictive control: In the shallows of the deepc, in: 2019 18th European Control Conference (ECC), IEEE. pp. 307–312.
- Deng, Z., Yang, K., Shen, W., Shi, Y., 2023. Cooperative platoon formation of connected and autonomous vehicles: Toward efficient merging coordination at unsignalized intersections. *IEEE Transactions on Intelligent Transportation Systems*.
- Dey, K.C., Yan, L., Wang, X., Wang, Y., Shen, H., Chowdhury, M., Yu, L., Qiu, C., Soundararaj, V., 2015. A review of communication, driver characteristics, and controls aspects of cooperative adaptive cruise control (cacc). *IEEE Transactions on Intelligent Transportation Systems* 17, 491–509.
- Ettinger, S., Cheng, S., Caine, B., Liu, C., Zhao, H., Pradhan, S., Chai, Y., Sapp, B., Qi, C.R., Zhou, Y., et al., 2021. Large scale interactive motion forecasting for autonomous driving: The waymo open motion dataset, in: *Proceedings of the IEEE/CVF International Conference on Computer Vision*, pp. 9710–9719.
- Feng, S., Zhang, Y., Li, S.E., Cao, Z., Liu, H.X., Li, L., 2019. String stability for vehicular platoon control: Definitions and analysis methods. *Annual Reviews in Control* 47, 81–97.
- Feng, Y., Yu, C., Liu, H.X., 2018. Spatiotemporal intersection control in a connected and automated vehicle environment. *Transportation Research Part C: Emerging Technologies* 89, 364–383.
- Gao, C., Wang, Z., He, X., Dong, H., 2021. Fault-tolerant consensus control for multiagent systems: An encryption-decryption scheme. *IEEE Transactions on Automatic Control* 67, 2560–2567.
- Guo, Q., Li, L., Ban, X.J., 2019. Urban traffic signal control with connected and automated vehicles: A survey. *Transportation research part C: emerging technologies* 101, 313–334.
- He, B.Y., Chow, J.Y., 2019. Optimal privacy control for transport network data sharing. *Transportation Research Procedia* 38, 792–811.
- Jin, I.G., Orosz, G., 2014. Dynamics of connected vehicle systems with delayed acceleration feedback. *Transportation Research Part C: Emerging Technologies* 46, 46–64.
- Li, K., Ni, W., Emami, Y., Shen, Y., Severino, R., Pereira, D., Tovar, E., 2019. Design and implementation of secret key agreement for platoon-based vehicular cyber-physical systems. *ACM Transactions on Cyber-Physical Systems* 4, 1–20.
- Li, S.E., Zheng, Y., Li, K., Wu, Y., Hedrick, J.K., Gao, F., Zhang, H., 2017. Dynamical modeling and distributed control of connected and automated vehicles: Challenges and opportunities. *IEEE Intelligent Transportation Systems Magazine* 9, 46–58.
- Ma, Z., Zhang, T., Liu, X., Li, X., Ren, K., 2019. Real-time privacy-preserving data release over vehicle trajectory. *IEEE transactions on vehicular technology* 68, 8091–8102.
- Nekouei, E., Pirani, M., Sandberg, H., Johansson, K.H., 2021. A randomized filtering strategy against inference attacks on active steering control systems. *IEEE Transactions on Information Forensics and Security* 17, 16–27.
- Nekouei, E., Sandberg, H., Skoglund, M., Johansson, K.H., 2022. A model randomization approach to statistical parameter privacy. *IEEE Transactions on Automatic Control*.
- Orosz, G., 2016. Connected cruise control: modelling, delay effects, and nonlinear behaviour. *Vehicle System Dynamics* 54, 1147–1176.
- Pan, D., Ding, D., Ge, X., Han, Q.L., Zhang, X.M., 2022. Privacy-preserving platooning control of vehicular cyber-physical systems with saturated inputs. *IEEE Transactions on Systems, Man, and Cybernetics: Systems*.
- Punzo, V., Borzacchiello, M.T., Ciuffo, B., 2011. On the assessment of vehicle trajectory data accuracy and application to the next generation simulation (ngsim) program data. *Transportation Research Part C: Emerging Technologies* 19, 1243–1262.
- Qin, G., Deng, S., Luo, Q., Sun, J., Kerivin, H., 2022. Toward privacy-aware multimodal transportation: Convergence to network equilibrium under differential privacy. Available at SSRN 4244002.
- Shen, M., He, C.R., Molnar, T.G., Bell, A.H., Orosz, G., 2023. Energy-efficient connected cruise control with lean penetration of connected vehicles. *IEEE Transactions on Intelligent Transportation Systems* 24, 4320–4332.
- Sun, X., Ye, Q., Hu, H., Wang, Y., Huang, K., Wo, T., Xu, J., 2023. Synthesizing realistic trajectory data with differential privacy. *IEEE Transactions on Intelligent Transportation Systems*.
- Sun, Z., Zan, B., Ban, X.J., Gruteser, M., 2013. Privacy protection method for fine-grained urban traffic modeling using mobile sensors. *Transportation Research Part B: Methodological* 56, 50–69.
- Swaroop, D., Hedrick, J.K., 1996. String stability of interconnected systems. *IEEE transactions on automatic control* 41, 349–357.
- Tan, C., Yang, K., 2024. Privacy-preserving adaptive traffic signal control in a connected vehicle environment. *Transportation Research Part C: Emerging Technologies* 158, 104453.
- Tan, C., Yao, J., Tang, K., et al., 2022. Joint estimation of multi-phase traffic demands at signalized intersections based on connected vehicle trajectories. *arXiv preprint arXiv:2210.10516*.
- Teunissen, P., 1990. Nonlinear least squares.
- Tilg, G., Yang, K., Menendez, M., 2018. Evaluating the effects of automated vehicle technology on the capacity of freeway weaving sections. *Transportation Research Part C: Emerging Technologies* 96, 3–21.
- Tsao, M., Gopalakrishnan, K., Yang, K., Pavone, M., 2023. Differentially private stochastic convex optimization for network routing applications, in: 2023 62nd IEEE Conference on Decision and Control (CDC), IEEE. pp. 7475–7482.
- Tsao, M., Yang, K., Gopalakrishnan, K., Pavone, M., 2022a. Private location sharing for decentralized routing services, in: 2022 IEEE 25th International Conference on Intelligent Transportation Systems (ITSC), IEEE. pp. 2479–2486.
- Tsao, M., Yang, K., Zoepf, S., Pavone, M., 2022b. Trust but verify: Cryptographic data privacy for mobility management. *IEEE Transactions on Control of Network Systems* 9, 50–61.
- Van Erven, T., Harremoës, P., 2014. Rényi divergence and kullback-leibler divergence. *IEEE Transactions on Information Theory* 60, 3797–3820.

- Wang, J., Lian, Y., Jiang, Y., Xu, Q., Li, K., Jones, C.N., 2022a. Distributed deep-lcc for cooperatively smoothing large-scale mixed traffic flow via connected and automated vehicles. arXiv preprint arXiv:2210.13171 .
- Wang, J., Zheng, Y., Chen, C., Xu, Q., Li, K., 2021. Leading cruise control in mixed traffic flow: System modeling, controllability, and string stability. IEEE Transactions on Intelligent Transportation Systems 23, 12861–12876.
- Wang, J., Zheng, Y., Li, K., Xu, Q., 2023a. Deep-lcc: Data-enabled predictive leading cruise control in mixed traffic flow. IEEE Transactions on Control Systems Technology .
- Wang, J., Zheng, Y., Xu, Q., Li, K., 2022b. Data-driven predictive control for connected and autonomous vehicles in mixed traffic, in: 2022 American Control Conference (ACC), IEEE. pp. 4739–4745.
- Wang, Q., Dong, H., Ju, F., Zhuang, W., Lv, C., Wang, L., Song, Z., 2023b. Adaptive leading cruise control in mixed traffic considering human behavioral diversity. IEEE Transactions on Intelligent Transportation Systems .
- Willems, J.C., Rapisarda, P., Markovsky, I., De Moor, B.L., 2005. A note on persistency of excitation. Systems & Control Letters 54, 325–329.
- Wills, A., Ninness, B., 2008. On gradient-based search for multivariable system estimates. IEEE Transactions on Automatic Control 53, 298–306.
- Woo, S., Skabardonis, A., 2021. Flow-aware platoon formation of connected automated vehicles in a mixed traffic with human-driven vehicles. Transportation research part C: emerging technologies 133, 103442.
- Xiao, L., Wang, M., Schakel, W., van Arem, B., 2018. Unravelling effects of cooperative adaptive cruise control deactivation on traffic flow characteristics at merging bottlenecks. Transportation research part C: emerging technologies 96, 380–397.
- Yang, K., Guler, S.I., Menendez, M., 2016. Isolated intersection control for various levels of vehicle technology: Conventional, connected, and automated vehicles. Transportation Research Part C: Emerging Technologies 72, 109–129.
- Zhang, K., Chen, K., Li, Z., Chen, J., Zheng, Y., 2023. Privacy-preserving data-enabled predictive leading cruise control in mixed traffic. IEEE Transactions on Intelligent Transportation Systems .
- Zhang, Y., Bai, Y., Hu, J., Cao, D., Wang, M., 2022. Memory-anticipation strategy to compensate for communication and actuation delays for strings-stable platooning. IEEE Transactions on Intelligent Vehicles 8, 1145–1155.
- Zhang, Y., Bai, Y., Wang, M., Hu, J., 2020. Cooperative adaptive cruise control with robustness against communication delay: An approach in the space domain. IEEE Transactions on Intelligent Transportation Systems 22, 5496–5507.
- Zhou, J., Yan, L., Yang, K., 2024. Enhancing system-level safety in mixed-autonomy platoon via safe reinforcement learning. arXiv preprint arXiv:2401.11148 .
- Zhou, J., Yu, H., 2022. Safety critical control of mixed-autonomy traffic via a single autonomous vehicle, in: 2022 IEEE 25th International Conference on Intelligent Transportation Systems (ITSC), IEEE. pp. 3089–3094.
- Zhou, J., Zhu, F., 2021. Analytical analysis of the effect of maximum platoon size of connected and automated vehicles. Transportation Research Part C: Emerging Technologies 122, 102882.

A. Linearized Discrete-Time System Dynamics for Mixed-Autonomy Traffic

We linearize and discretize the continuous mixed-traffic platoon system presented in Eq. (3) to formulate a discrete-time linear time-invariant (LTI) system characterized by a positive time interval $T_{\text{step}} > 0$. Notice that the linearization and time discretization are performed locally on each HV.

First, we linearize the nonlinear car-following model for HDV $i \in \Omega_{\mathcal{H}}$ in Eq. (1) using the first-order Taylor expansion around the equilibrium state $x_i^* = [s_i^*, v^*]$, which satisfies $\mathbb{F}_{\kappa_i}(s_i^*, v^*, v^*) = 0$ with v^* specified by the head vehicle. This process yields the following linearized dynamics:

$$\begin{cases} \dot{s}_i^{\text{err}}(t) = v_{i-1}^{\text{err}}(t) - v_i^{\text{err}}(t), \\ \dot{v}_i^{\text{err}}(t) = \alpha_1 s_i^{\text{err}}(t) - \alpha_2 v_i^{\text{err}}(t) + \alpha_3 v_{i-1}^{\text{err}}(t), \end{cases} \quad (50)$$

where $\alpha_1 = \frac{\partial F}{\partial s}$, $\alpha_2 = \frac{\partial F}{\partial s} - \frac{\partial F}{\partial v}$, $\alpha_3 = \frac{\partial F}{\partial s}$, $s_i^{\text{err}} = s_i - s^*$, $v_i^{\text{err}} = v_i - v^*$ are the error states of the system. The state vector for vehicle i is denoted by $x_i^{\text{err}}(t) = [s_i^{\text{err}}(t), v_i^{\text{err}}(t)]$.

Then using the linear dynamics of CAV in Eq. (2) and the linearized HDV dynamics in Eq. (50), the nonlinear system dynamics in Eq. (3) can be transformed into the linear form:

$$\dot{x}^{\text{err}}(t) = Ax^{\text{err}}(t) + Bu(t) + H\epsilon(t), \quad (51)$$

where $A \in \mathbb{R}^{2n \times 2n}$, $B, H \in \mathbb{R}^{2n \times m}$. $\epsilon(t)$ represents the velocity deviation of the head vehicle, denoted by $v_0^{\text{err}}(t)$, which is treated as an exogenous disturbance in the system.

We next transform the continuous-time LTI system represented in Eq. (51) to a discrete-time LTI system formulated as:

$$\begin{cases} x^{\text{err}}(k+1) = A_d x^{\text{err}}(t_s) + B_d u(t_s) + H_d \epsilon(t_s), \\ y(t_s) = C_d x^{\text{err}}(t_s), \end{cases} \quad (52)$$

where $A_d = e^{AT_{\text{step}}} \in \mathbb{R}^{2n \times 2n}$ represents the state transition matrix of the discrete-time system, $B_d = \int_0^{T_{\text{step}}} e^{At} B dt \in \mathbb{R}^{2n \times m}$ is the control input matrix, $H_d = \int_0^{T_{\text{step}}} e^{At} H dt \in \mathbb{R}^{2n}$ corresponds to the disturbance input matrix, and $C_d = C \in \mathbb{R}^{(n+m) \times 2n}$ is the output matrix. These matrices collectively define the dynamics of the discrete-time LTI system.

Additionally, in scenarios where each HDV within the mixed traffic is equipped with a privacy filter as described in Eq. (10), the dynamics of the system are modified to:

$$\begin{cases} x^{\text{err}}(k+1) = A_d x^{\text{err}}(t_s) + B_d u(t_s) + H_d \epsilon(t_s), \\ \bar{x}_i^{\text{err}}(t_s) = \Gamma_i (x_i^{\text{err}}(t_s) + x^*, v_{i-1}^{\text{err}}(t_s) + v^*, \kappa_i) - x^*, i \in \Omega_H, \\ y(t_s) = C_d x'(t_s), \end{cases} \quad (53)$$

where $x'(t_s) = \left\{ \{ \bar{x}_i^{\text{err}}(t) \}_{i \in \Omega_H}, \{ x_j^{\text{err}}(t) \}_{j \in \Omega_C} \right\}$ represents a composite state comprising pseudo states from HDVs and true states from CAVs.

B. Non-Parametric Representation for DeePC Using Fundamental Lemma

The non-parametric system representation is based on Willems' fundamental lemma (Willems et al., 2005) using the Hankel matrix defined as follows:

$$\mathcal{H}_L(\omega) := \begin{bmatrix} \omega_{\text{Hankel}}(1) & \omega_{\text{Hankel}}(2) & \cdots & \omega_{\text{Hankel}}(T_{\text{ini}} - L + 1) \\ \omega_{\text{Hankel}}(2) & \omega_{\text{Hankel}}(3) & \cdots & \omega_{\text{Hankel}}(T_{\text{ini}} - L + 2) \\ \vdots & \vdots & \ddots & \vdots \\ \omega_{\text{Hankel}}(L) & \omega_{\text{Hankel}}(L + 1) & \cdots & \omega_{\text{Hankel}}(T_{\text{ini}}) \end{bmatrix}, \quad (54)$$

where $\omega_{\text{Hankel}} = \text{col}(\omega_{\text{Hankel}}(1), \omega_{\text{Hankel}}(2), \dots, \omega_{\text{Hankel}}(T_{\text{ini}}))$ denotes the signal sequence with length T_{ini} and $L (L \leq T_{\text{ini}})$ represents the number of rows in the Hankel matrix. If the Hankel Matrix in Eq. (54) is of full rank, then the signal sequence ω_{Hankel} is *persistently exciting* of order L . Then the fundamental lemma is given as follows:

Lemma 4 (Fundamental Lemma). *Consider a controllable LTI system and assume the input sequence u^d to be persistently exciting of order $L + N$. Then, (u^s, y^s) is a length L input/output trajectory of the system if and only if there exists $g \in \mathbb{R}^{T-L+1}$ such that*

$$\begin{bmatrix} \mathcal{H}_L(u^d) \\ \mathcal{H}_L(y^d) \end{bmatrix} g = \begin{bmatrix} u^s \\ y^s \end{bmatrix}. \quad (55)$$

Using the fundamental Lemma in Eq. (55), the system behaviors can be represented in a non-parametric way. In the mixed-autonomy traffic, the signal sequence includes the pre-collected sequence of control input $u^d \in \mathbb{R}^{m(T_{\text{ini}}+N)}$ and the pre-collected sequence of system output $y^d \in \mathbb{R}^{m(T_{\text{ini}}+N)}$ with length $T_{\text{ini}} + N$ for systems in Eq. (52) and Eq. (53), which can be represented as:

$$u_{[1, T_{\text{ini}}+N]}^d = \begin{bmatrix} u^d(1) \\ \vdots \\ u^d(T_{\text{ini}} + N) \end{bmatrix}, \epsilon_{[1, T_{\text{ini}}+N]}^d = \begin{bmatrix} \epsilon^d(1) \\ \vdots \\ \epsilon^d(T_{\text{ini}} + N) \end{bmatrix}, y_{[1, T_{\text{ini}}+N]}^d = \begin{bmatrix} y^d(1) \\ \vdots \\ y^d(T_{\text{ini}} + N) \end{bmatrix}. \quad (56)$$

The above data sequences are divided into ‘‘past data’’ with length T_{ini} and ‘‘future data’’ with length N , which are transformed into the form of Hankel Matrix, respectively:

$$\begin{bmatrix} U_p \\ U_f \end{bmatrix} := \mathcal{H}_{T_{\text{ini}}+N}(u^d), \quad \begin{bmatrix} E_p \\ E_f \end{bmatrix} := \mathcal{H}_{T_{\text{ini}}+N}(\epsilon^d), \quad \begin{bmatrix} Y_p \\ Y_f \end{bmatrix} := \mathcal{H}_{T_{\text{ini}}+N}(y^d), \quad (57)$$

where U_p, E_p, Y_p denote the first T_{ini} rows of the Hankel metrics $\mathcal{H}_{T_{\text{ini}}+N}(u^d), \mathcal{H}_{T_{\text{ini}}+N}(\epsilon^d), \mathcal{H}_{T_{\text{ini}}+N}(y^d)$, U_f, E_f, Y_f represent the last N rows of the Hankel metrics $\mathcal{H}_{T_{\text{ini}}+N}(u^d), \mathcal{H}_{T_{\text{ini}}+N}(\epsilon^d), \mathcal{H}_{T_{\text{ini}}+N}(y^d)$.

At the timestep t , given the following sequences:

$$\begin{cases} u_{\text{ini}} = \text{col}(u(t - T_{\text{ini}}), u(t - T_{\text{ini}} + 1), \dots, u(t - 1)), \\ u = \text{col}(u(t), u(t + 1), \dots, u(t + N - 1)), \\ \epsilon_{\text{ini}} = \text{col}(\epsilon(t - T_{\text{ini}}), \epsilon(t - T_{\text{ini}} + 1), \dots, \epsilon(t - 1)), \\ \epsilon = \text{col}(\epsilon(t), \epsilon(t + 1), \dots, \epsilon(t + N - 1)), \\ y_{\text{ini}} = \text{col}(y(t - T_{\text{ini}}), y(t - T_{\text{ini}} + 1), \dots, y(t - 1)), \\ y = \text{col}(y(t), y(t + 1), \dots, y(t + N - 1)), \end{cases} \quad (58)$$

where u_{ini} is the control signal sequence for the last T_{ini} steps and u denotes predicted sequence with time horizon N (Similar for $\epsilon_{\text{ini}}, \epsilon$ and y_{ini}, y). Then utilizing the fundamental lemma in Eq. (55), we have the behavior representation for the mixed-autonomy traffic:

$$\begin{bmatrix} U_p \\ E_p \\ Y_p \\ U_f \\ E_f \\ Y_f \end{bmatrix} g = \begin{bmatrix} u_{\text{ini}} \\ \epsilon_{\text{ini}} \\ y_{\text{ini}} \\ u \\ \epsilon \\ y \end{bmatrix}. \quad (59)$$

C. Derivation of Head-to-Tail Transfer Function

First, with the true parameters for HDV i , we perform Laplace transform for the linearized car-following dynamics in Eq. (50) with true parameters as:

$$\begin{cases} V_i^{\text{err}} = \frac{\alpha_3 s + \alpha_1}{s^2 + \alpha_2 s + \alpha_1} V_{i-1}^{\text{err}}, \\ S_i^{\text{err}} = \frac{1}{s} \left(1 - \frac{\alpha_3 s + \alpha_1}{s^2 + \alpha_2 s + \alpha_1} \right) V_{i-1}^{\text{err}}, \end{cases} \quad (60)$$

where $V_i^{\text{err}}(s), V_{i-1}^{\text{err}}(s)$ and S_i^{err} denote the Laplace transform of the error state $v_i^{\text{err}}, v_{i-1}^{\text{err}}$ and s_i^{err} , respectively.

Then, we derive the formulation of the local transfer function for HDV with true parameters. After the Laplace transform, the local velocity transfer function for HDV i and $i - 1$ can be written as:

$$K(s) = \frac{V_i^{\text{err}}}{V_{i-1}^{\text{err}}} = \frac{\alpha_3 s + \alpha_1}{s^2 + \alpha_2 s + \alpha_1}. \quad (61)$$

For the convenience of computation, the Laplace transform of spacing S_i^{err} can also be represented by the function of V_i^{err} as $S_i^{\text{err}} = \frac{1}{s} \left(\frac{1}{K(s)} - 1 \right) V_i^{\text{err}}$.

Similarly, for HDV i with a privacy filter, the Laplace transform of pseudo states \bar{S}_i^{err} and \bar{V}_i^{err} can be represented by the Laplace transform of preceding vehicle velocity as V_{i-1}^{err} as:

$$\begin{cases} \bar{V}_i^{\text{err}} = \frac{\bar{\alpha}_3 s + \bar{\alpha}_1}{s^2 + \bar{\alpha}_2 s + \bar{\alpha}_1} V_{i-1}^{\text{err}}, \\ \bar{S}_i^{\text{err}} = \frac{1}{s} \left(1 - \frac{\bar{\alpha}_3 s + \bar{\alpha}_1}{s^2 + \bar{\alpha}_2 s + \bar{\alpha}_1} \right) V_{i-1}^{\text{err}}. \end{cases} \quad (62)$$

And we also have the local transfer function for pseudo state $\bar{K}(s) = \frac{\bar{V}_i^{\text{err}}}{V_{i-1}^{\text{err}}} = \frac{\bar{\alpha}_3 s + \bar{\alpha}_1}{s^2 + \bar{\alpha}_2 s + \bar{\alpha}_1}$. Similarly, for the convenience of calculation, we have $\bar{S}_i^{\text{err}} = \frac{1}{s} \left(\frac{1}{\bar{K}(s)} - 1 \right) \bar{V}_i^{\text{err}}$.

Then we give the details of the local transfer function for the CAV. In our scenario, partial HDVs are equipped with privacy filters to conceal their driving behavior so that the information CAV (index i_{cav}) received has been distorted. The velocity dynamics for CAV utilizes Eq. (2) and Eq. (9), and the Laplace transform for the velocity dynamics are as follows:

$$\dot{v}_{i_{\text{cav}}}(t) = \mu_{i_{\text{cav}}} s_{i_{\text{cav}}}^{\text{err}}(t) + k_{i_{\text{cav}}} v_{i_{\text{cav}}}^{\text{err}}(t) + \sum_{i \in \Omega_p \cup \Omega_f \setminus \tilde{\Omega}_p \cup \tilde{\Omega}_f} (\mu_i s_i^{\text{err}}(t) + k_i v_i^{\text{err}}(t)) + \sum_{j \in \tilde{\Omega}_p \cup \tilde{\Omega}_f} (\mu_j \bar{s}_j^{\text{err}}(t) + k_j \bar{v}_j^{\text{err}}(t)), \quad (63)$$

$$\left(s - k_{i_{\text{cav}}} - \frac{\mu_{i_{\text{cav}}}}{s} \right) V_{i_{\text{cav}}}^{\text{err}} = \sum_{i \in \Omega_p \cup \Omega_f \setminus \tilde{\Omega}_p \cup \tilde{\Omega}_f} (\mu_i S_i^{\text{err}} + k_i V_i^{\text{err}}) + \sum_{j \in \tilde{\Omega}_p \cup \tilde{\Omega}_f} (\mu_j \bar{S}_j^{\text{err}} + k_j \bar{V}_j^{\text{err}}). \quad (64)$$

Let the local velocity transfer function for CAV be represented as $G(s) = \frac{V_{i_{\text{cav}}}^{\text{err}}}{V_{i_{\text{cav}}-1}^{\text{err}}}$. Using the local transfer function for HDV $K(s)$ in Eq. (61) and the local transfer function for CAV $G(s)$, we can rewrite Eq. (62) by replacing V_i^{err} with $V_{i_{\text{cav}}}^{\text{err}}$ (Laplace transform of head vehicle velocity) for the following vehicles and preceding vehicles of the CAV as

$$\begin{cases} V_i^{\text{err}} = \frac{1}{G(s)K^{i_{\text{cav}}-i-1}(s)} V_{i_{\text{cav}}}^{\text{err}}, \\ S_i^{\text{err}} = \frac{1 - K(s)}{sG(s)K^{i_{\text{cav}}-i}(s)} V_{i_{\text{cav}}}^{\text{err}}, \end{cases} \quad i \in \Omega_p \setminus \tilde{\Omega}_p, \quad (65)$$

$$\begin{cases} V_i^{\text{err}} = K^{i-i_{\text{cav}}}(s) V_{i_{\text{cav}}}^{\text{err}}, \\ S_i^{\text{err}} = \frac{1}{s} (1 - K(s)) K^{i-i_{\text{cav}}-1}(s) V_{i_{\text{cav}}}^{\text{err}}, \end{cases} \quad i \in \Omega_f \setminus \tilde{\Omega}_f. \quad (66)$$

Using the local transfer function for HDV with pseudo parameters $\bar{K}(s)$ and the local transfer function for CAV $G(s)$, we can also rewrite Eq. (62) by replacing \bar{V}_i^{err} with $V_{i_{\text{cav}}}^{\text{err}}$ for the following vehicles and preceding vehicles of the CAV as

$$\begin{cases} \bar{V}_j^{\text{err}} = \bar{K}(s) V_{j-1}^{\text{err}} = \frac{\bar{K}(s)}{G(s)K^{i_{\text{cav}}-j}(s)} V_{i_{\text{cav}}}^{\text{err}}, \\ \bar{S}_j^{\text{err}} = \frac{1 - \bar{K}(s)}{sG(s)K^{i_{\text{cav}}-j}(s)} V_{i_{\text{cav}}}^{\text{err}}, \end{cases} \quad j \in \tilde{\Omega}_p, \quad (67)$$

$$\begin{cases} \bar{V}_j^{\text{err}} = \bar{K}(s)K^{j-i_{\text{cav}}-1}(s)V_{i_{\text{cav}}}^{\text{err}}, \\ \bar{S}_j^{\text{err}} = \frac{1}{s}(1 - \bar{K}(s))K^{j-i_{\text{cav}}-1}(s)V_{i_{\text{cav}}}^{\text{err}}, \end{cases} \quad j \in \bar{\Omega}_F. \quad (68)$$

Then integrating Eq. (68) and Eq. (67) into Eq. (64), we have:

$$R(s) = W_1(s) + W_2(s)/G(s) + W_3(s) + W_4(s)/G(s), \quad (69)$$

where

$$\begin{aligned} R(s) &= \frac{s^2 - k_{i_{\text{cav}}}s - \mu_{i_{\text{cav}}}}{s}, \\ W_1(s) &= \sum_{i \in \Omega_p \setminus \bar{\Omega}_p} \left(\mu_i \frac{1 - K(s)}{sK^{i_{\text{cav}}-i}(s)} + k_i \frac{1}{K^{i_{\text{cav}}-i-1}(s)} \right), \\ W_2(s) &= \sum_{i \in \Omega_p \setminus \bar{\Omega}_p} \left(\mu_i \frac{1}{s}(1 - K(s))K^{i-i_{\text{cav}}-1}(s) + k_i K^{i-i_{\text{cav}}}(s) \right), \\ W_3(s) &= \sum_{j \in \bar{\Omega}_p} \left(\mu_j \frac{1 - \bar{K}(s)}{sK^{i_{\text{cav}}-j}(s)} + k_j \frac{\bar{K}(s)}{K^{i_{\text{cav}}-j}(s)} \right), \\ W_4(s) &= \sum_{j \in \bar{\Omega}_p} \left(\mu_j \frac{1}{s}(1 - \bar{K}(s))K^{j-i_{\text{cav}}-1}(s) + k_j \bar{K}(s)K^{j-i_{\text{cav}}-1}(s) \right). \end{aligned}$$

Then $G(s)$ can be represented by:

$$G(s) = \frac{W_2(s) + W_4(s)}{R(s) + W_1(s) + W_3(s)}. \quad (70)$$